

1 **Impact of low-pressure systems on winter heavy air pollution in the northwest Sichuan Basin, China**

2 Guicai Ning<sup>1,4</sup>, Shigong Wang<sup>2,1</sup>, Steve Hung Lam Yim<sup>3,4,5</sup>, Jixiang Li<sup>1</sup>, Yuling Hu<sup>1</sup>, Ziwei Shang<sup>1</sup>, Jinyan Wang<sup>1</sup>,  
3 Jiaxin Wang<sup>2</sup>

4 <sup>1</sup>The Gansu Key Laboratory of Arid Climate Change and Reducing Disaster, College of Atmospheric Sciences,  
5 Lanzhou University, Lanzhou 730000, China

6 <sup>2</sup>Key Laboratory of Education Bureau of Sichuan Province for Mountain Environmental Meteorology and Public  
7 Health, School of Atmospheric Sciences, Chengdu University of Information Technology, Chengdu 610225, China

8 <sup>3</sup>Department of Geography and Resource Management, The Chinese University of Hong Kong, Hong Kong, China

9 <sup>4</sup>The Institute of Environment, Energy and Sustainability, The Chinese University of Hong Kong, Hong Kong, China

10 <sup>5</sup>Stanley Ho Big Data Decision Analytics Research Centre, The Chinese University of Hong Kong, Shatin, N.T., Hong  
11 Kong, China

12 Correspondence to: Shigong Wang ([wangsg@cuit.edu.cn](mailto:wangsg@cuit.edu.cn), [wangsg@lzu.edu.cn](mailto:wangsg@lzu.edu.cn))

13 **Abstract**

14 The cities of Chengdu, Deyang, and Mianyang in the northwest Sichuan Basin are part of a rapidly developing  
15 urban agglomeration adjoining the eastern slopes of the Tibetan Plateau. Heavy air pollution events have frequently  
16 occurred over the cities in recent decade, but the effects of meteorological conditions on these pollution events are  
17 unclear. We explored the effects of weather systems on winter heavy air pollution from 1 January 2006 to 31 December  
18 2012 and from 1 January 2014 to 28 February 2017. Ten heavy air pollution events occurred during the research period  
19 and eight of these took place while the region was affected by a dry low-pressure system at 700 hPa. When the urban  
20 agglomeration was in front of the low-pressure system and the weather conditions were controlled by a warm southerly  
21 air flow, and a strong temperature inversion appeared above the atmospheric boundary layer acting as a lid. Forced by  
22 this strong inversion layer, the local secondary circulation was confined within the atmospheric boundary layer and the  
23 horizontal wind speed in the lower troposphere was low. As a result, vertical mixing and horizontal dispersion in the  
24 atmosphere were poor, favoring the formation of heavy air pollution events. After the low-pressure system had  
25 transited over the region, the weather conditions in the urban agglomeration were controlled by a dry and cold air flow  
26 from the northwest at 700 hPa. The strong inversion layer gradually dissipated, the secondary circulation enhanced and

27 uplifted, and the horizontal wind speed in the lower troposphere also increased, resulting in a sharp decrease in the  
28 concentration of air pollutants. The strong inversion layer above the atmospheric boundary layer induced by the  
29 low-pressure system at 700 hPa thus played a key role in the formation of heavy air pollution during the winter months  
30 in this urban agglomeration. This study provides scientific insights for forecasting heavy air pollution in this region of  
31 China.

## 32 **1 Introduction**

33 Air quality, especially the occurrence of heavy air pollution events, is not only strongly affected by excessive  
34 emission of air pollutants, but is also closely associated with meteorological conditions, including atmospheric  
35 circulations, weather systems, structures of atmospheric boundary layer, and the corresponding meteorological  
36 parameters (**Deng et al., 2014;Gu and Yim, 2016;Li et al., 2015;Wei et al., 2011;Ye et al., 2016;Zhang et al.,**  
37 **2012a**). The total amount of pollutants emitted in a particular period of time is usually stable in China (**Wu et al.,**  
38 **2017**), but there are large differences in the concentrations of air pollutants, indicating that the meteorological  
39 conditions have an important role in modulating concentrations of ambient air pollutants (**Gao et al., 2011;Hu et al.,**  
40 **2014;Ji et al., 2014;Ji et al., 2012;Wang et al., 2010;Wang et al., 2009;Yang et al., 2011**).

41 Weather systems control the ability of the atmosphere to disperse pollutants and thus provide the primary driving  
42 force for variations in regional air pollution (**Chen et al., 2008;Ye et al., 2016**). Leśniok et al. (2010) reported that the  
43 atmosphere was stagnant and that the concentrations of near-ground air pollutants increased significantly in Upper  
44 Silesia, Poland during periods with an anticyclonic circulation. By contrast, when a cyclonic circulation prevailed,  
45 causing an inflow of fresh air masses from regions with lower levels of pollution, the concentrations of air pollutants  
46 decreased. As synoptic-scale high-pressure ridges at 500 hPa transit across Utah, accompanied by warm advection  
47 above valleys, the stability of the atmosphere is increased and favors the formation of persistent pools of cold air,  
48 resulting in deterioration in air quality (**Whiteman et al., 2014**).

49 Many studies have been carried out on the impact of weather systems on air quality in China. Bei et al. (2016)

50 classified typical synoptic situations and evaluated their contributions to air quality in the Guanzhong Basin, China.  
51 They found that an inland high-pressure system at 850 hPa resulted in temperature inversion, low horizontal wind  
52 speed and a shallow atmospheric boundary layer, which favor the formation of heavy air pollution. Weather systems  
53 have significantly impact on the transport of air pollutants. Luo et al. (2018) reported that the trans-boundary air  
54 pollution and the pollutant concentration in Hong Kong increased when a tropical cyclones is approaching. During  
55 winter, floating dust particles over northwestern China can be carried downstream to northern China by the prevailing  
56 northwesterly winds at 700 hPa, where they mix with anthropogenic pollution to form a regional haze (**Tao et al.,**  
57 **2012;Tao et al., 2014**). Changes in weather systems also significantly influence air quality. Shallowing of the East  
58 Asian trough and weakening of the Siberian high-pressure in winter can induce weak horizontal advection and vertical  
59 convection in the lower troposphere, reducing the height of the boundary layer in the Beijing–Tianjin–Hebei region  
60 and favoring the formation of haze (**Zhang et al., 2016**).

61 The deep Sichuan Basin to the east of the Tibetan Plateau has a maximum elevation difference >2000 m, and is  
62 ranked fourth in China for heavy air pollution after the Beijing–Tianjin–Hebei region, the Yangtze River Delta, and the  
63 Pearl River Delta (**Tian et al., 2017;Zhang et al., 2012b**). The complex terrain leads to unique weather systems that  
64 affect air quality in this region (**Chen et al., 2014;Huang et al., 2017**). Low-pressure systems, such as a southwest  
65 vortex and low trough, are often formed at 700 hPa due to the dynamic and thermodynamic effects of the Tibetan  
66 Plateau (**Wang and Tan, 2014;Yu et al., 2016**) and have different characteristics in different seasons. They are warm  
67 and moist low-pressure systems in summer and autumn and have crucial effects on local precipitation (**Feng et al.,**  
68 **2016;Peng and Cheng, 1992**); much work has been carried out in an attempt to understand the impacts of these  
69 low-pressure systems on precipitation (**Chen et al., 2015;Fu et al., 2011;Kuo et al., 1986;Kuo et al., 1988;Ni et al.,**  
70 **2017**). In winter and spring, however, these low-pressure systems are both dry and cold (**Feng et al., 2016**). No  
71 attempt has previously been made to investigate the association between air quality and these dry and cold  
72 low-pressure systems.

73 Chengdu, Deyang, and Mianyang, have undergone rapid development to form an urban agglomeration in the  
74 northwest Sichuan Basin. This urban agglomeration lies close to the eastern slopes of Tibetan Plateau, and is affected  
75 by low-pressure systems moving east from the plateau (**Feng et al., 2016**). Heavy air pollution events have frequently  
76 occurred over there in recent decade. Number of days with exceedance of Grade II standards (**MEP, 2012**) is more  
77 than 150 days each year in Chengdu (**Ning et al., 2018**). Most previous studies have investigated the basic  
78 characteristics of air pollution (**Chen and Xie, 2012;Chen et al., 2014;Luo et al., 2001;Ning et al., 2018;Tao et al.,**  
79 **2013a;Tao et al., 2013b;Zhang et al., 2017**) and the related meteorological parameters (**He et al., 2017;Li et al.,**  
80 **2015;Liao et al., 2017;Zeng and Zhang, 2017**). However, the influencing mechanism of dry low-pressure system on  
81 heavy air pollution events has yet to be comprehensively explored. The main purpose of this study was to statistically  
82 analyze the relationships between low-pressure systems and winter heavy air pollution events in this urban  
83 agglomeration, and to explore the physical mechanisms involved in the formation of winter heavy air pollution. This  
84 study can deepen our understanding of the meteorological causes of heavy air pollution events in winter, and provide  
85 scientific insights that can be used by local governments to take effective measures to mitigate air pollution.

86 This paper is organized as follows. The data and methods are described in Section 2. Section 3 provides a  
87 statistical analysis of the relationships between the low-pressure systems and winter heavy air pollution. Section 4  
88 illustrates the physical mechanisms of the effect of weather systems on air pollution and our conclusions are  
89 summarized in Section 5.

## 90 **2 Data and methods**

### 91 **2.1 Air quality data**

92 Air pollution in the Sichuan Basin during the winter months is mainly caused by particulate matter (**Ning et al.,**  
93 **2018**). The Chinese Ministry of Environmental Protection (MEP) currently monitors particles with diameters  $\leq 2.5 \mu\text{m}$   
94 ( $\text{PM}_{2.5}$ ) and particles with diameters  $\leq 10 \mu\text{m}$  ( $\text{PM}_{10}$ ). We studied heavy air pollution events occurring during the winter  
95 months in Chengdu, Deyang, and Mianyang in the northwest Sichuan Basin (**Fig. 1**). We selected pollution events with

96 a daily PM<sub>10</sub> mean concentration  $\geq 350 \mu\text{g m}^{-3}$  from 1 January 2006 to 31 December 2012 and from 1 January 2014 to  
97 28 February 2017. The third revision of the “Ambient Air Quality Standard” (AAQS) (GB3095-2012) was released on  
98 February 29<sup>th</sup>, 2012, replacing the old “Ambient Air Quality Standard” (AAQS) (GB3095-1996) and PM<sub>2.5</sub> was  
99 adopted into the AAQS in China since 2013. The air quality monitoring stations needed to be updated and the data of  
100 air pollutants monitored in the three cities existed missing measurement during 2013. Thus, the winter heavy pollution  
101 events during 2013 have not been analyzed in this paper. Moreover, the PM<sub>10</sub> daily mean concentration from 1 January  
102 2014 to 28 February 2017 refers to the 24-hour average concentration of PM<sub>10</sub> from 00:00 BST (Beijing Standard  
103 Time, i.e., Coordinate Universal Time (UTC) +8 h) to 24:00 BST on the current day based on the new “Ambient Air  
104 Quality Standard” (AAQS) (GB3095-2012). However, based on the old “Ambient Air Quality Standard” (AAQS)  
105 (GB3095-1996), the PM<sub>10</sub> daily mean concentration from 1 January 2006 to 31 December 2012 refers to the 24-hour  
106 average concentration of PM<sub>10</sub> from 12:00 BST on the previous day to 12:00 BST on the current day. Hourly  
107 concentrations of PM<sub>2.5</sub>, sulfur dioxide (SO<sub>2</sub>), nitrogen dioxide (NO<sub>2</sub>), carbon monoxide (CO), and ozone (O<sub>3</sub>) were  
108 also measured in the three cities from 1 January 2014 to 28 February 2017. These above air quality data were collected  
109 from the MEP website (<http://datacenter.mep.gov.cn/index>).

## 110 **2.2 Meteorological data**

### 111 **(1) ERA-Interim daily data**

112 To analyze the weather systems at 700 hPa, and the dynamic and thermodynamic conditions in the lower  
113 troposphere, the temperature, the geopotential, the vertical velocity, and the u and v components of wind during the  
114 study period were obtained from the ERA-Interim daily dataset (0.125° × 0.125° grids) from 950 to 500 hPa for a total  
115 of 14 vertical layers (with a vertical separation of 25 hPa from 950 to 775 hPa and a vertical separation of 50 hPa from  
116 750 to 500 hPa). These meteorological data are available for 00:00, 06:00, 12:00, and 18:00 UTC and were collected  
117 from the website (<http://apps.ecmwf.int/datasets/data/interim-full-daily/levtype=pl/>). The height of the atmospheric  
118 boundary layer was obtained from the ERA-Interim daily dataset at the surface with a 3 h temporal resolution (00:00,

119 03:00, 06:00, 09:00, 12:00, 15:00, 18:00, and 21:00 UTC)  
120 (<http://apps.ecmwf.int/datasets/data/interim-full-daily/levtype=sfc/>) to explore the structure of the atmospheric  
121 boundary layer. This boundary layer height was defined as the level where the bulk Richardson number, based on the  
122 difference between quantities at that level and the lowest model level, reaches the critical value  $Ri_{cr} = 0.25$  (Beljaars,  
123 2006).

## 124 (2) Sounding data

125 Radiosonde measurements from launches at Wenjiang station (see Fig. 1) in Chengdu city (30.70 °N, 103.83 °E,  
126 elevation 541.0 m) at 08:00 and 20:00 BST were obtained from the University of Wyoming website  
127 (<http://weather.uwyo.edu/upperair/sounding.html>) and included the temperature, potential temperature, and horizontal  
128 wind. These data were used to investigate the dynamic and thermodynamic structure of the lower troposphere.

## 129 2.3 Quantitative measures of meteorological conditions

### 130 2.3.1 Lower tropospheric stability

131 The lower tropospheric stability (LTS) is defined as the difference in the potential temperature between 700 hPa  
132 and the surface (Slingo, 1987), and can be used to describe the thermodynamic state of the lower troposphere (Guo et  
133 al., 2016a;Guo et al., 2016b). The LTS can be used to quantitatively evaluate the vertical mixing of air pollutants in  
134 the lower troposphere:

$$135 \text{ LTS} = \theta_{700\text{hPa}} - \theta_{\text{surface}} \quad (1)$$

136 A large LTS represents a high degree of stability in the lower troposphere and indicates the potential for the weak  
137 vertical mixing of air pollutants.

### 138 2.3.2 The mean wind speed in the lower troposphere

139 Sichuan Basin belongs to a low wind speed zone in China due to its deep mountain-basin topography, and the  
140 wind speed in the mixing layer is often low and with small change magnitudes (Chen and Xie, 2012;Huang et al.,  
141 2017;Wang et al., 2018). For analyzing air quality in Sichuan Basin, the meteorological conditions in the lower

142 troposphere that can reflect ventilation should be considered. To quantitatively evaluate the horizontal dispersion of air  
143 pollutants in Sichuan Basin, the mean wind speed (MWS) in the lower troposphere was constructed based on the  
144 concept of ventilation coefficient (VC is a product of mixing layer height multiplied by average wind speed through  
145 the mixing height). In the eastern plains of China, the ventilation coefficient has been widely used to measure the  
146 capability of air pollutants' dispersion (**Deng et al., 2014;Lu et al., 2012;Tang et al., 2015**). The mean wind speed  
147 (MWS) in the lower troposphere was defined as:

$$148 \quad \text{MWS} = \frac{1}{h} \int_0^h V(z) dz \quad (2)$$

149 where h is the height above the ground at 700 hPa and  $V(z)$  is the wind speed in the lower troposphere. This can be  
150 simplified as follows:

$$151 \quad \text{MWS} = \frac{1}{h} \sum_{i=1}^n [V_i(z_i) + V_{i-1}(z_{i-1})] \cdot 0.5 \cdot \Delta z_i \quad (3)$$

152 where n is the number of vertical layers from the ground surface to 700 hPa isobaric layer (including the 700 hPa  
153 isobaric layer, and n is greater than 6 in general),  $V_i(z_i)$  is the wind speed in a vertical layer (when i=0 represents  
154 the wind speed at the ground surface and i=n represents the wind speed at 700 hPa), and  $\Delta z_i$  is the difference in  
155 height between the two adjacent vertical layers. A large value of MWS suggests strong horizontal dispersion of air  
156 pollutants.

### 157 **3 Heavy air pollution events and weather conditions**

#### 158 **3.1 Overview of the heavy air pollution events**

159 A total of ten heavy winter air pollution events occurred from 1 January 2006 to 31 December 2012 and from 1  
160 January 2014 to 28 February 2017 in the urban agglomeration of Chengdu, Deyang, and Mianyang. Nine events were  
161 accompanied by a low-pressure system at 700 hPa, and the low-pressure systems in eight events were dry and didn't

162 induce precipitation. This paper explores the impacts of dry low-pressure systems on the eight winter heavy air  
163 pollution events (see **Table 1** for a summary of these eight events).

164 **Table 1** shows that particulate matter was the primary pollutants during these eight heavy air pollution events. Six  
165 of the eight events were classified as persistent air pollution events. A “persistent” pollution event was defined by two  
166 or more consecutive days with daily PM<sub>10</sub> mean concentration  $\geq 250 \mu\text{g m}^{-3}$ , which is reported to be harmful to the  
167 health of local residents (**Chow et al., 2006;Guo et al., 2016c;Langrish et al., 2012;Lim et al., 2012**), and the longest  
168 duration was 10 days. Most of the heavy air pollution events had the characteristics of regional pollution, with five  
169 pollution events occurring in multiple cities. Two heavy air pollution events (events 6 and 7) occurred during the  
170 Spring Festival, with maximum daily mean PM<sub>10</sub> concentrations up to 403 and 562  $\mu\text{g m}^{-3}$  on the Chinese New Year  
171 Day. This suggests that the centralized letting-off of fireworks during the traditional Chinese Spring Festival,  
172 accompanied by poor conditions for the dispersion of air pollution, may lead to a sharp increase in the concentration of  
173 particulate pollutants near ground level within a short period of time (**Huang et al., 2012;Liao et al., 2017;Shi et al.,**  
174 **2011;Wang et al., 2007**).

### 175 **3.2 Weather systems and meteorological conditions during heavy air pollution events**

176 An analysis of the synoptic conditions showed that the urban agglomeration was affected by low-pressure systems  
177 (low vortex or low trough) at 700 hPa during periods of deteriorating air quality in the eight heavy air pollution events  
178 (**Fig. 2**). These studied areas were all located in front of low-pressure systems (east of low-pressure systems) and were  
179 controlled by a southerly warm air flow (**Fig. 2**). To explore the differences between these low-pressure systems and  
180 the background of winter atmospheric circulation over there, the anomalies of wind vectors and geopotential heights at  
181 700 hPa were calculated (**Fig. S1**). The calculation method is as follows: the averaged wind vectors and geopotential  
182 heights at 700 hPa during periods of deteriorating air quality in the above eight events subtracted from their winter  
183 mean values from 1 January 2006 to 31 December 2012 and from 1 January 2014 to 28 February 2017. As illustrated  
184 in **Fig. S1**, the anomalies of geopotential heights were negative in the northwest of the urban agglomeration during



185 periods of deteriorating air quality in these heavy air pollution events. As a result, this urban agglomeration was  
186 located in front of an anomalous cyclone and was controlled by a strong southerly anomaly wind (**Fig. S1**).

187 Weather systems can be characterized by their relative vorticity. A positive relative vorticity usually corresponds  
188 to a low-pressure system, whereas a negative relative vorticity usually represents a high-pressure system. Thus the  
189 relative vorticity at 700 hPa was analyzed during periods of both deteriorating and improving air quality (**Table 2**). As  
190 shown in **Table 2**, the relative vorticities at 700 hPa during periods of deteriorating air quality were all positive. This  
191 indicated that the study areas were located in front of low-pressure systems at 700 hPa. As a result, a southerly warm  
192 air flow dominated at 700 hPa and led to an increase in temperature above the atmospheric boundary layer, which  
193 increased atmospheric stability and favored the formation of an air pollution event. During periods of improving air  
194 quality, the relative vorticities at 700 hPa of six heavy air pollution events (except for events 6 and 7) were negative,  
195 showing that the low-pressure systems had transited across the study areas. These areas were thus controlled by a  
196 northerly dry, cold air flow at 700 hPa. As a consequence, the temperature above the atmospheric boundary layer  
197 decreased and the stability of the atmosphere weakened, which favored the vertical mixing of air pollutants.

198 To explore the impacts of low-pressure systems on the structure of the atmospheric boundary layer, the boundary  
199 layer height during periods of deteriorating and improving air quality were analyzed for each heavy air pollution event  
200 (**Table 3**). In most of the heavy air pollution events, the height of the boundary layer increased after the low-pressure  
201 system had passed across the study area. However, the increase in the height of the boundary layer was not as  
202 significant as that seen in Eastern China (**He et al., 2015; Ji et al., 2012; Leng et al., 2016; Qu et al., 2017; Quan et al.,**  
203 **2013**) and the boundary layer heights in air pollution events 3, and 4 decreased after transit of the low-pressure system.  
204 These results show that the effects of the transit of low-pressure systems at 700 hPa on the height of the boundary layer  
205 were weak, and the causes for the formation of these features will be discussed later. It is therefore difficult to explain  
206 the variations in the concentrations of air pollutants in the study areas by considering only the meteorological  
207 conditions within the boundary layer.

208 Previous studies have shown that the meteorological conditions above the boundary layer should also be  
209 considered (Guo et al., 2016a;Guo et al., 2016b;Slingo, 1987). Therefore an index of the MWS in the lower  
210 troposphere was proposed and this index, together with the LTS of the eight heavy air pollution events, were further  
211 investigated (Table 3). The differences in the potential temperature between 700 hPa and the surface during periods of  
212 deteriorating air quality in the eight events were all  $\geq 18.54$  K and the maximum value was 29.45 K, indicating that the  
213 lower troposphere was very stable. The MWS was  $\leq 4.22$  m s<sup>-1</sup> for all eight events, with a minimum of 1.91 m s<sup>-1</sup>.  
214 These results show that the low-pressure systems resulted in the stagnation of air in the lower troposphere. After the  
215 low-pressure systems had transited the study area, the lower tropospheric stability significantly decreased, with a  
216 maximum decrease in the LTS of up to -11.23 K, and the MWS increased. This showed that the arrival of a dry, cold  
217 air flow induced by the transit of the low-pressure system significantly weakened the stability of the lower troposphere  
218 and increased the wind speed, improving air quality.

219 In events 6 and 7, however, although the study areas were still located in front of the low-pressure system and the  
220 capacity for dispersion had not yet improved, the concentrations of particulate matter began to sharply decrease before  
221 the transit of the low-pressure system. Both of these events occurred during the Chinese Spring Festival. After the  
222 Chinese New Year Day, the letting-off of fireworks stopped and the emission of air pollutants was significantly  
223 reduced, resulting in a sharp decrease in the concentration of particulate matter (Liao et al., 2017;Shi et al.,  
224 2011;Wang et al., 2007). The decrease in the magnitude of the daily mean concentration of PM<sub>10</sub> in event 7 was up to  
225 350  $\mu\text{g m}^{-3}$ . These eight heavy air pollution events in the northwest Sichuan Basin can therefore be categorized into  
226 two types based on their date of occurrence. The two heavy air pollution events (6 and 7) occurring during the Chinese  
227 Spring Festival were categorized as Spring Festival excessive emission heavy air pollution events. The other six events  
228 (events 1–5 and 8) were categorized as normal heavy air pollution events.

#### 229 **4 Impacts of low-pressure systems on heavy air pollution events**

230 To further explore the mechanism involved in the formation of heavy air pollution events, with a particular

231 emphasis on the effect of low-pressure systems on air quality, a typical event was selected from the eight events  
232 described in the preceding section. The variations in air quality and the dynamic and thermodynamic conditions in the  
233 lower troposphere of the selected event were analyzed. Additionally, the impacts of Spring Festival excessive emission  
234 on heavy air pollution events were also investigated.

#### 235 **4.1 The influencing mechanism of low-pressure systems on heavy air pollution events**

236 Heavy air pollution event 8 occurred from 1 January 2017 to 6 January 2017 (Table 3) and the most polluted area  
237 was Chengdu. The maximum daily mean concentrations of  $PM_{2.5}$  and  $PM_{10}$  occurred on 5 January 2017. The  
238 maximum  $PM_{10}$  daily mean concentration in Chengdu was up to  $480 \mu g m^{-3}$ . The concentrations of particulate matter  
239 increased sharply (**Fig. 3**) from 00:00 BST on 3 January 2017 to 00:00 BST on 5 January 2017 and the concentrations  
240 of nitrogen dioxide and carbon monoxide also showed an increasing trend. Since 12:00 BST on 5 January 2017, the  
241 concentrations of particulate matter decreased significantly (**Fig. 3**).

242 **Fig. 4** shows the weather maps at 700 hPa during event 8. **Fig. 4a** shows that there was no low-pressure system at  
243 700 hPa over the urban agglomeration at 02:00 BST on 2 January and there was a dry, cold air flow from the northwest.  
244 Soon, as shown in **Fig. 4b**, a low trough was generated at 700 hPa on the west side of the urban agglomeration at 14:00  
245 BST on 2 January 2017, which showed the beginning of low-pressure system causing air pollution. This trough later  
246 developed and was enhanced, and the lifespan of this low-pressure system was about 3 days. The urban agglomeration  
247 was still located at the front of the trough and was controlled by a warm, moist air flow from the southwest until 02:00  
248 BST on 5 January 2017 (**Fig. 4b** and **4c**). The concentrations of particulate matter in the urban agglomeration increased  
249 sharply and the air quality deteriorated. The trough developed further and a low vortex was formed, which transited  
250 across over the study area at 02:00 BST on 5 January 2017 (**Fig. 4d**). The urban agglomeration was then located  
251 behind the low vortex and was controlled by a northerly dry, cold air flow (**Fig. 4d**), which illustrated the  
252 meteorological conditions in the end of air pollution event. As a result, the air pollutants were rapidly dispersed.

253 The west–east vertical cross-sections of the 24-hour change in temperature and wind vectors (u and w) in the most

254 polluted area (30.75 °N) (**Fig. 5**) and the vertical profiles of temperature and horizontal wind speed (**Fig. 6**) were  
255 analyzed to investigate the effects of the low-pressure system on the dynamic and thermodynamic dispersion of air  
256 pollutants in the lower troposphere.

257 **Fig.4b** and **4c** shows that the urban agglomeration was located in front of the low-pressure system and was  
258 controlled by a southerly warm air flow. There was a descending motion between the top of the boundary layer and  
259 500 hPa (**Fig. 5a** and **5b**). Under the effects of warm advection and descending motion, a warming center appeared  
260 between 800 and 650 hPa (**Fig. 5a–c**) and the maximum increase in the 24-hour temperature was up to 10 °C (**Fig. 6a**).  
261 Weak cooling occurred below 800 hPa, a strong temperature inversion appeared between 775 and 650 hPa (**Fig. 6a**),  
262 and the stability of the lower troposphere increased. The urban agglomeration was dominated by the low-pressure  
263 system for a long time and a long-lasting strong temperature inversion was therefore induced and maintained above the  
264 boundary layer. This was different from the temperature inversion that is often seen within the boundary layer in  
265 Eastern China (**Ji et al., 2012;Li and Chan, 2016;Li et al., 2012;Wang et al., 2014;Zhang and Niu, 2016**). The  
266 temperature inversion acted as a lid over the boundary layer, suppressing the dispersion of air pollutants. This lid effect  
267 restrained vertical mixing in the atmosphere and the local secondary circulation was therefore confined in the boundary  
268 layer, with its center located at about 850 hPa (**Fig. 5a–c**). The horizontal wind speed below 800 hPa was  $\leq 2 \text{ m s}^{-1}$  (**Fig.**  
269 **6b**). These results indicate that vertical mixing and horizontal dispersion were weak, causing accumulation of air  
270 pollutants at the ground level. The concentrations of particulate matter then sharply increased to their peak value (**Fig.**  
271 **3**), generating a heavy air pollution event.

272 A low vortex and trough at 700 hPa transited across the urban agglomeration and a northwesterly dry, cold air flow  
273 prevailed (**Fig. 4d**). Under the influence of the cold air flow, a cooling center appeared between 800 and 650 hPa (**Fig.**  
274 **5d**), whereas the air temperature increased below 800 hPa (**Fig. 5d**). As a result, the stability in the lower troposphere  
275 was weakened and the strong inversion layer gradually disappeared (**Fig. 6a**). The lid effect above the boundary layer  
276 also disappeared, resulting in an increase in the local secondary circulation, the center of which was uplifted to 700

277 hPa (**Fig. 5d**). The horizontal wind speed below 800 hPa also increased (**Fig. 6b**). The air pollutants were able to  
278 disperse over a larger space and the vertical mixing and horizontal dispersion were significantly improved. The air  
279 quality improved and the heavy air pollution event ended.

280 To verify whether the mechanism involved in the formation of event 8 is used for the others heavy air pollution  
281 events, the vertical profiles of temperature and horizontal wind speed in events 1-7 (**Fig. 7**) were explored during the  
282 periods of both the low-pressure system controlling and transited over this urban agglomeration. Similar to the event 8,  
283 a strong temperature inversion appeared over the study area between 800 and 650 hPa (**Fig. 7a**) when the urban  
284 agglomeration was located in the front of low-pressure system and was controlled by a southerly warm air flow at 700  
285 hPa. Meanwhile, the horizontal wind speed was low below 800 hPa; the wind speed at all levels below 850 hPa was  $\leq 2$   
286  $\text{m s}^{-1}$  (**Fig. 7c**). After the low-pressure system had transited across the urban agglomeration, the strong inversion layer  
287 above the boundary layer gradually disappeared (**Fig. 7b**), and the horizontal wind speed in the lower troposphere  
288 increased (**Fig. 7d**). Therefore, the influencing mechanism of low-pressure system on heavy air pollution events is  
289 common in this urban agglomeration.

290 Additionally, the anomalies of west-to-east vertical cross-section of 24-hour temperature change and wind vectors  
291 (synthesized by u and w) (**Fig. S2**), and the anomalies of temperature vertical profiles (**Fig. S3**) were also analyzed to  
292 further investigate the influencing mechanism of low-pressure system on heavy air pollution events. **Fig. S2** shows that  
293 anomalous warming appeared above the atmospheric boundary layer, while anomalous cooling was observed within  
294 the boundary layer when the urban agglomeration was located in front of low-pressure system and was controlled by a  
295 southerly warm air flow at 700 hPa. This vertical structure of the anomalies of 24-hour temperature change led to an  
296 increase in the stability of the lower troposphere. As illustrated in **Fig. S3**, the positive anomalies of temperature  
297 between 1500 m and 3000 m above the ground level increased significantly with height. The maximum value of  
298 positive anomalies appeared at about 3000 m and was up to 9 °C. These features revealed that a strong temperature  
299 inversion existed above the boundary layer and suppressed the vertical exchange of atmosphere. As a result, the

300 anomalous secondary circulation was also confined in the boundary layer, with its center located at about 925 hPa (**Fig.**  
301 **S2**). These results of anomalies analysis were consistent with the above analysis for real-time data, and further proved  
302 that the influencing mechanism of low-pressure system on heavy air pollution events is credible.

303 From **Fig.6** and **Fig.7**, we also found some interesting features that the effects of the transit of low-pressure  
304 systems at 700 hPa on the meteorological factors within the boundary layer were weak. These features may be related  
305 to its deep mountain-basin topography (**Fig. 1**). Under the effects of the deep mountain-basin topography, wind speed  
306 in the boundary layer is often low and with small change magnitudes (**Chen and Xie, 2012;Huang et al., 2017;Wang**  
307 **et al., 2018**), and cold air induced by the transit of low-pressure systems is usually difficult to reach in the ground layer  
308 faster (**Fig. 5**). As a result, the increase magnitudes of wind speed (**Fig. 6b, Fig. 7 c and 7d**) and the change  
309 magnitudes of temperature (**Fig. 6a, Fig. 7a and 7b**) were very small in the boundary layer after the low-pressure  
310 system at 700 hPa passed. Especially for events 3 and 4, the wind speed decreased and a temperature inversion formed  
311 in the boundary layer. These characteristics of the wind and temperature profiles in the boundary layer were the key  
312 factors leading to the evolution of boundary layer height as shown in **Table 3**.

#### 313 **4.2 Impacts of Spring Festival excessive emission on heavy air pollution events**

314 **Table 1** shows that events 6 and 7 occurred during the Chinese Spring Festival when the concentration of  
315 particulate matter increased sharply. Low concentrations of gaseous pollutants were found throughout these two events,  
316 however, which may be related to a reduction in production or the shut-down of factories, as well as lower numbers of  
317 vehicles during the week-long Spring Festival (**Liao et al., 2017**). The centralized letting-off of fireworks during the  
318 Chinese Spring Festival played an important part in the sharp increase in the concentrations of particulate matter  
319 (**Huang et al., 2012;Liao et al., 2017;Shi et al., 2011;Wang et al., 2007**). We investigated the impacts of Spring  
320 Festival excessive emission on events 6 and 7.

321 It's noteworthy that the emission of air pollutants increased sharply during this period of deteriorating air quality  
322 for events 6 and 7 due to the centralized letting-off of fireworks during the Chinese Spring Festival. What's more,

323 under the effects of low-pressure system, the strong temperature inversion appeared above the atmospheric boundary  
324 layer (**Fig. 7a**) and the horizontal wind speed was low below 800 hPa (**Fig. 7c**). The combination of excessive  
325 emissions with poor dispersion conditions resulted in the maximum daily concentrations of PM<sub>10</sub> occurring on the  
326 Chinese New Year Day (**Table 1**). The maximum daily mean PM<sub>10</sub> concentration of eight heavy air pollution events  
327 occurred in event 7 and was up to 562 μg m<sup>-3</sup> (**Table 1**). This shows that the excessive emissions during the short  
328 Chinese Spring Festival were able to increase the peak concentrations of particulate matter. Thus, the centralized  
329 letting-off of fireworks in the Chinese Spring Festival combined with the impacts of low-pressure system were the  
330 main causes of these two events in this region of China.

331 Unlike in the normal heavy air pollution events, the concentrations of particulate matter began to decrease sharply  
332 in event 6 and 7 before the low-pressure system transited over the urban agglomeration (**Fig. 8a** and **8b**), when the  
333 strong temperature inversion was still present above the atmospheric boundary layer (**Fig. 10**), the local secondary  
334 circulation was still confined in the atmospheric boundary layer (**Fig. 9a** and **9b**) and the capacity for dispersion has  
335 not yet improved significantly (**Table 3**). To explore the causes of the sharp decrease in PM<sub>10</sub> concentration for these  
336 two events, the effects of fireworks on air quality in Chengdu during Chinese New Year (CNY) from 2013 to 2017  
337 have been investigated. The results showed that time-variations of PM<sub>10</sub> concentration during CNY were similar in  
338 these five years, even though their meteorological conditions were different. As illustrated in **Fig. S4**, PM<sub>10</sub>  
339 concentration increased sharply during the periods of the letting-off of fireworks in CNY, and began to decrease  
340 significantly after the letting-off of fireworks stopped. These results were consistent with the changes of particulate  
341 pollutant concentrations during CNY in other cities of China  
342 ([http://www.zhb.gov.cn/gkml/hbb/qt/201702/t20170201\\_395336.htm](http://www.zhb.gov.cn/gkml/hbb/qt/201702/t20170201_395336.htm)). It is a common phenomenon that PM<sub>10</sub>  
343 concentrations decreased sharply after the letting-off of fireworks stopped during CNY. Additionally, the diurnal  
344 variations of the differences of averaged PM<sub>10</sub> concentration in Chengdu between during in the periods of the  
345 letting-off of fireworks in CNY (defined as the period from 12:00 BST on the Eve of CNY to 12:00 BST on 1 Lunar

346 January) and 5 days before the letting-off fireworks, and between during 5 days after the letting-off of fireworks in  
347 CNY and in the periods of the letting-off of fireworks from 2013 to 2017 have been also analyzed (**Fig. S5**) to evaluate  
348 the effects of excessive emission about fireworks on air quality in a better way. The letting-off of fireworks during  
349 CNY was observed to have a significant effect on the air quality in Chengdu. Especially during 5 days after the  
350 letting-off of fireworks stopped, production was reduced, factories were shut-down and the numbers of vehicles were  
351 lower due to the week-long holiday of CNY (**Liao et al., 2017**). As a result, the maximum decrease in the magnitude of  
352  $PM_{10}$  concentration was more than  $220 \mu g m^{-3}$  and occurred at night from 00:00 BST to 06:00 BST (**Fig. S5**) which  
353 corresponded to the period of the centralized letting-off of fireworks. Based on the above analysis results, we  
354 concluded that the sharp decreases in  $PM_{10}$  concentration for events 6 and 7 were mainly attributable to the significant  
355 reduction in emissions induced by the letting-off of fireworks stopped and the week-long holiday of CNY. This  
356 indicated that these two events were strongly dependent on emissions.

## 357 **5 Conclusions and discussions**

358 We investigated the relationships between low-pressure systems and winter heavy air pollution events in the  
359 urban agglomeration of Chengdu, Deyang, and Mianyang in the northwest Sichuan Basin and explored the influence of  
360 dry and cold low-pressure systems on winter air quality.

361 A total of ten heavy winter air pollution events occurred in the urban agglomeration from 1 January 2006 to 31  
362 December 2012 and from 1 January 2014 to 28 February 2017. The meteorological causes of eight of these air  
363 pollution events were attributed to dry low-pressure systems (trough and low vortex) at 700 hPa. The schematic  
364 diagram in **Fig. 11** shows that a strong temperature inversion appeared above the atmospheric boundary layer because  
365 the urban agglomeration was located in front of low-pressure system at 700 hPa and was controlled by a warm  
366 southerly air flow. This strong inversion layer acted as a lid over the boundary layer and suppressed the dispersion of  
367 air pollutants, confining the local secondary circulation within the atmospheric boundary layer. The horizontal wind  
368 speed in the lower troposphere was low. As a result, the space available for the vertical and horizontal dispersion of air



369 pollutants was small. The concentrations of air pollutants increased to their peak values, resulting in heavy air  
370 pollution events.

371 After the low-pressure system had transited across the urban agglomeration, the strong inversion layer above the  
372 boundary layer gradually disappeared, resulting in an increase and uplift of the secondary circulation and an increase in  
373 the horizontal wind speed in the lower troposphere. The space available for the vertical and horizontal dispersion of air  
374 pollutants increased and the concentrations of air pollutants decreased sharply, ending the heavy air pollution event.  
375 The centralized letting-off of fireworks during the Chinese Spring Festival was one of the main causes of the heavy air  
376 pollution events in this region of China.

377 The urban agglomeration studied here, which is flanked by the eastern slopes of the Tibetan Plateau, is sensitive  
378 to low-pressure systems moving east from the plateau (**Feng et al., 2016**). The complex terrain forms local secondary  
379 circulations, which have a significant impact on air quality (**Chen et al., 2009;Liu et al., 2009;Miao et al., 2015**). We  
380 found that the intensity and altitude of the local secondary circulations were markedly affected by the low-pressure  
381 system and changes in circulation affected the local air quality. The mechanism of influence of the low-pressure  
382 system on the local secondary circulation requires further elaboration using numerical simulation. The centralized  
383 letting-off of fireworks during the Chinese Spring Festival significantly affected the air quality (**Huang et al.,**  
384 **2012;Liao et al., 2017;Shi et al., 2011;Wang et al., 2007**), especially during some of the heavy air pollution events in  
385 the urban agglomeration, although the impact of fireworks on air quality was remarkably different depending on the  
386 dispersion conditions (**Li et al., 2006**). Sensitivity research should therefore be carried out using models coupled with  
387 detailed meteorological and chemical processes to quantitatively examine the impacts of the centralized emission of air  
388 pollutants from the Chinese Spring Festival on local air quality.

389 **Competing interests**

390 The authors declare that they have no conflict of interest.

391 **Acknowledgements**

392 This work was supported by the National Natural Science Foundation of China (91644226, 41575138), the National  
393 Key Research Project of China-Strategy on Black Carbon Reduction and Evaluation of the Health Effects of Climate  
394 Change (2016YFA0602004), the Improvement on Competitiveness in Hiring New Faculties Fund (2013/14) of The  
395 Chinese University of Hong Kong and the Vice-Chancellor's Discretionary Fund of The Chinese University of Hong  
396 Kong (4930744). We would like to thank the following departments for the provided data, the Ministry of  
397 Environmental Protection of the People's Republic of China, the European Centre for Medium-Range Weather  
398 Forecasts, the University of Wyoming and the China Meteorological Administration. Anonymous reviewers who  
399 provided comments and suggestions are gratefully acknowledged.

400 **References**

- 401 Bei, N., Li, G., Huang, R. J., Cao, J., Meng, N., Feng, T., Liu, S., Zhang, T., Zhang, Q., and Molina, L. T.: Typical synoptic  
402 situations and their impacts on the wintertime air pollution in the Guanzhong basin, China[J], *Atmos. Chem. Phys.*, 16,  
403 7373-7387, <https://doi.org/10.5194/acp-16-7373-2016>, 2016.
- 404 Beljaars, A.: Chapter 3: Turbulent transport and interactions with the surface. Part IV: Physical Processes, IFS  
405 Documentation, Operational implementation 12 September 2006 Cy31r1 31, ECMWF, Shinfield Park[J], Reading, RG2  
406 9AX, England, 2006.
- 407 Chen, Y., Li, Y., and Zhao, T.: Cause analysis on eastward movement of Southwest China vortex and its induced heavy  
408 rainfall in South China[J], *Adv Meteorol.*, 2015, 22, <https://doi.org/10.1155/2015/481735>, 2015.
- 409 Chen, Y., and Xie, S.: Temporal and spatial visibility trends in the Sichuan Basin, China, 1973 to 2010[J], *Atmos. Res.*, 112,  
410 25-34, <https://doi.org/10.1016/j.atmosres.2012.04.009>, 2012.
- 411 Chen, Y., Xie, S., Luo, B., and Zhai, C.: Characteristics and origins of carbonaceous aerosol in the Sichuan Basin, China[J],  
412 *Atmos. Environ.*, 94, 215-223, <https://doi.org/10.1016/j.atmosenv.2014.05.037>, 2014.
- 413 Chen, Y., Zhao, C., Zhang, Q., Deng, Z., Huang, M., and Ma, X.: Aircraft study of mountain chimney effect of Beijing,  
414 China[J], *J. Geophys. Res.*, 114, n/a-n/a, <https://doi.org/10.1029/2008JD010610>, 2009.
- 415 Chen, Z. H., Cheng, S. Y., Li, J. B., Guo, X. R., Wang, W. H., and Chen, D. S.: Relationship between atmospheric pollution  
416 processes and synoptic pressure patterns in northern China[J], *Atmos. Environ.*, 42, 6078-6087,  
417 <https://doi.org/10.1016/j.atmosenv.2008.03.043>, 2008.

418 Chow, J. C., Watson, J. G., Mauderly, J. L., Costa, D. L., Wyzga, R. E., Vedal, S., Hidy, G. M., Altshuler, S. L., Marrack, D.,  
419 Heuss, J. M., Wolff, G. T., Arden Pope Iii, C., and Dockery, D. W.: Health effects of fine particulate air pollution: Lines  
420 that connect[J], *J. Air Waste Manage. Assoc.*, 56, 1368-1380, <https://doi.org/10.1080/10473289.2006.10464545>, 2006.

421 Deng, T., Wu, D., Deng, X., Tan, H., Li, F., and Liao, B.: A vertical sounding of severe haze process in Guangzhou area[J],  
422 *Sci. China Earth Sci.*, 57, 2650-2656, 10.1007/s11430-014-4928-y, 2014.

423 Feng, X., Liu, C., Fan, G., Liu, X., and Feng, C.: Climatology and structures of southwest vortices in the NCEP Climate  
424 Forecast System Reanalysis[J], *J. Climate.*, 29, 7675-7701, <https://doi.org/10.1175/jcli-d-15-0813.1>, 2016.

425 Fu, S., Sun, J., Zhao, S., and Li, W.: The energy budget of a southwest vortex with heavy rainfall over south China[J], *Adv.*  
426 *Atmos. Sci.*, 28, 709-724, <https://doi.org/10.1007/s00376-010-0026-z>, 2011.

427 Gao, Y., Liu, X., Zhao, C., and Zhang, M.: Emission controls versus meteorological conditions in determining aerosol  
428 concentrations in Beijing during the 2008 Olympic Games[J], *Atmos. Chem. Phys.*, 11, 12437-12451,  
429 <https://doi.org/10.5194/acp-11-12437-2011>, 2011.

430 Gu, Y., and Yim, S. H. L.: The air quality and health impacts of domestic trans-boundary pollution in various regions of  
431 China[J], *Environ. Int.*, 97, 117-124, <https://doi.org/10.1016/j.envint.2016.08.004>, 2016.

432 Guo, J., Deng, M., Lee, S. S., Wang, F., Li, Z., Zhai, P., Liu, H., Lv, W., Yao, W., and Li, X.: Delaying precipitation and  
433 lightning by air pollution over the Pearl River Delta. Part I: Observational analyses[J], *J. Geophys. Res.-Atmos.*, 121,  
434 6472-6488, <https://doi.org/10.1002/2015JD023257>, 2016a.

435 Guo, J., Miao, Y., Zhang, Y., Liu, H., Li, Z., Zhang, W., He, J., Lou, M., Yan, Y., Bian, L., and Zhai, P.: The climatology of  
436 planetary boundary layer height in China derived from radiosonde and reanalysis data[J], *Atmos. Chem. Phys.*, 16,  
437 13309-13319, <https://doi.org/10.5194/acp-16-13309-2016>, 2016b.

438 Guo, Y., Zeng, H., Zheng, R., Li, S., Barnett, A. G., Zhang, S., Zou, X., Huxley, R., Chen, W., and Williams, G.: The  
439 association between lung cancer incidence and ambient air pollution in China: A spatiotemporal analysis[J], *Environ.*  
440 *Res.*, 144, 60-65, <https://doi.org/10.1016/j.envres.2015.11.004>, 2016c.

441 He, H., Tie, X., Zhang, Q., Liu, X., Gao, Q., Li, X., and Gao, Y.: Analysis of the causes of heavy aerosol pollution in Beijing,  
442 China: A case study with the WRF-Chem model[J], *Particuology*, 20, 32-40,  
443 <https://doi.org/10.1016/j.partic.2014.06.004>, 2015.

444 He, J., Gong, S., Yu, Y., Yu, L., Wu, L., Mao, H., Song, C., Zhao, S., Liu, H., Li, X., and Li, R.: Air pollution characteristics  
445 and their relation to meteorological conditions during 2014–2015 in major Chinese cities[J], *Environ. Pollut.*, 223,  
446 484-496, <https://doi.org/10.1016/j.envpol.2017.01.050>, 2017.

447 Hu, X.-M., Ma, Z., Lin, W., Zhang, H., Hu, J., Wang, Y., Xu, X., Fuentes, J. D., and Xue, M.: Impact of the Loess Plateau on  
448 the atmospheric boundary layer structure and air quality in the North China Plain: A case study[J], *Sci. Total Environ.*,  
449 499, 228-237, <https://doi.org/10.1016/j.scitotenv.2014.08.053>, 2014.

450 Huang, K., Zhuang, G., Lin, Y., Wang, Q., Fu, J. S., Zhang, R., Li, J., Deng, C., and Fu, Q.: Impact of anthropogenic  
451 emission on air quality over a megacity – revealed from an intensive atmospheric campaign during the Chinese Spring  
452 Festival[J], *Atmos. Chem. Phys.*, 12, 11631-11645, <https://doi.org/10.5194/acp-12-11631-2012>, 2012.

453 Huang, Q., Cai, X., Song, Y., and Zhu, T.: Air stagnation in China (1985–2014): climatological mean features and trends[J],  
454 Atmos. Chem. Phys., 17, 7793-7805, <https://doi.org/10.5194/acp-17-7793-2017>, 2017.

455 Ji, D., Li, L., Wang, Y., Zhang, J., Cheng, M., Sun, Y., Liu, Z., Wang, L., Tang, G., Hu, B., Chao, N., Wen, T., and Miao, H.:  
456 The heaviest particulate air-pollution episodes occurred in northern China in January, 2013: Insights gained from  
457 observation[J], Atmos. Environ., 92, 546-556, <https://doi.org/10.1016/j.atmosenv.2014.04.048>, 2014.

458 Ji, D., Wang, Y., Wang, L., Chen, L., Hu, B., Tang, G., Xin, J., Song, T., Wen, T., Sun, Y., Pan, Y., and Liu, Z.: Analysis of  
459 heavy pollution episodes in selected cities of northern China[J], Atmos. Environ., 50, 338-348,  
460 <https://doi.org/10.1016/j.atmosenv.2011.11.053>, 2012.

461 Kuo, Y.-H., Cheng, L., and Anthes, R. A.: Mesoscale analyses of the Sichuan flood catastrophe, 11–15 July 1981[J], Mon.  
462 Wea. Rev., 114, 1984-2003, [https://doi.org/10.1175/1520-0493\(1986\)114<1984:maotsf>2.0.co;2](https://doi.org/10.1175/1520-0493(1986)114<1984:maotsf>2.0.co;2), 1986.

463 Kuo, Y.-H., Cheng, L., and Bao, J.-W.: Numerical simulation of the 1981 Sichuan flood. Part I: Evolution of a mesoscale  
464 southwest vortex[J], Mon. Wea. Rev., 116, 2481-2504,  
465 [https://doi.org/10.1175/1520-0493\(1988\)116<2481:nsotsf>2.0.co;2](https://doi.org/10.1175/1520-0493(1988)116<2481:nsotsf>2.0.co;2), 1988.

466 Langrish, J. P., Li, X., Wang, S., Lee, M. M. Y., Barnes, G. D., Miller, M. R., Cassee, F. R., Boon, N. A., Donaldson, K., Li, J.,  
467 Li, L., Mills, N. L., Newby, D. E., and Jiang, L.: Reducing personal exposure to particulate air pollution improves  
468 cardiovascular health in patients with coronary heart disease[J], Environ Health Perspect., 120, 367-372,  
469 <https://doi.org/10.1289/ehp.1103898>, 2012.

470 Leng, C., Duan, J., Xu, C., Zhang, H., Wang, Y., Wang, Y., Li, X., Kong, L., Tao, J., Zhang, R., Cheng, T., Zha, S., and Yu, X.:  
471 Insights into a historic severe haze event in Shanghai: synoptic situation, boundary layer and pollutants[J], Atmos.  
472 Chem. Phys., 16, 9221-9234, <https://doi.org/10.5194/acp-16-9221-2016>, 2016.

473 Leśniok, M., Małarzewski, L., and Niedźwiedz, T.: Classification of circulation types for Southern Poland with an  
474 application to air pollution concentration in Upper Silesia[J], Phys. Chem. Earth Parts A B C., 35, 516-522,  
475 <https://doi.org/10.1016/j.pce.2009.11.006>, 2010.

476 Li, L., and Chan, P. W.: LIDAR observation and numerical simulation of vortex/wave shedding at the eastern runway  
477 corridor of the Hong Kong international airport[J], Meteorol. Appl., 23, 379-388, <https://doi.org/10.1002/met.1562>,  
478 2016.

479 Li, L., Li, J., Xin, L., Li, H., and Wei, Q.: Analysis of atmospheric air pollution of Beijing City in Spring Festival period[J],  
480 China Environ. Sci, 26, 537-541 (in Chinese), [http://manu36.magtech.com.cn/Jweb\\_zghjkkx/CN/2006](http://manu36.magtech.com.cn/Jweb_zghjkkx/CN/2006).

481 Li, Y., Chen, Q., Zhao, H., Wang, L., and Tao, R.: Variations in PM<sub>10</sub>, PM<sub>2.5</sub> and PM<sub>1.0</sub> in an urban area of the Sichuan Basin  
482 and their relation to meteorological factors[J], Atmosphere., 6, 150, 2015.

483 Li, Y., Yan, J., and Sui, X.: Tropospheric temperature inversion over central China[J], Atmos. Res., 116, 105-115,  
484 <https://doi.org/10.1016/j.atmosres.2012.03.009>, 2012.

485 Liao, T., Wang, S., Ai, J., Gui, K., Duan, B., Zhao, Q., Zhang, X., Jiang, W., and Sun, Y.: Heavy pollution episodes, transport  
486 pathways and potential sources of PM<sub>2.5</sub> during the winter of 2013 in Chengdu (China)[J], Sci. Total Environ., 584-585,  
487 1056-1065, <https://doi.org/10.1016/j.scitotenv.2017.01.160>, 2017.

488 Lim, S. S., Vos, T., Flaxman, A. D., Danaei, G., Shibuya, K., Adair-Rohani, H., AlMazroa, M. A., Amann, M., Anderson, H.  
489 R., Andrews, K. G., Aryee, M., Atkinson, C., Bacchus, L. J., Bahalim, A. N., Balakrishnan, K., Balmes, J., Barker-Collo,  
490 S., Baxter, A., Bell, M. L., Blore, J. D., Blyth, F., Bonner, C., Borges, G., Bourne, R., Boussinesq, M., Brauer, M.,  
491 Brooks, P., Bruce, N. G., Brunekreef, B., Bryan-Hancock, C., Bucello, C., Buchbinder, R., Bull, F., Burnett, R. T., Byers,  
492 T. E., Calabria, B., Carapetis, J., Carnahan, E., Chafe, Z., Charlson, F., Chen, H., Chen, J. S., Cheng, A. T.-A., Child, J.  
493 C., Cohen, A., Colson, K. E., Cowie, B. C., Darby, S., Darling, S., Davis, A., Degenhardt, L., Dentener, F., Des Jarlais,  
494 D. C., Devries, K., Dherani, M., Ding, E. L., Dorsey, E. R., Driscoll, T., Edmond, K., Ali, S. E., Engell, R. E., Erwin, P.  
495 J., Fahimi, S., Falder, G., Farzadfar, F., Ferrari, A., Finucane, M. M., Flaxman, S., Fowkes, F. G. R., Freedman, G.,  
496 Freeman, M. K., Gakidou, E., Ghosh, S., Giovannucci, E., Gmel, G., Graham, K., Grainger, R., Grant, B., Gunnell, D.,  
497 Gutierrez, H. R., Hall, W., Hoek, H. W., Hogan, A., Hosgood, H. D., Hoy, D., Hu, H., Hubbell, B. J., Hutchings, S. J.,  
498 Ibeanusi, S. E., Jacklyn, G. L., Jasrasaria, R., Jonas, J. B., Kan, H., Kanis, J. A., Kassebaum, N., Kawakami, N., Khang,  
499 Y.-H., Khatibzadeh, S., Khoo, J.-P., Kok, C., Laden, F., Lalloo, R., Lan, Q., Lathlean, T., Leasher, J. L., Leigh, J., Li, Y.,  
500 Lin, J. K., Lipshultz, S. E., London, S., Lozano, R., Lu, Y., Mak, J., Malekzadeh, R., Mallinger, L., Marcenes, W.,  
501 March, L., Marks, R., Martin, R., McGale, P., McGrath, J., Mehta, S., Memish, Z. A., Mensah, G. A., Merriman, T. R.,  
502 Micha, R., Michaud, C., Mishra, V., Hanafiah, K. M., Mokdad, A. A., Morawska, L., Mozaffarian, D., Murphy, T.,  
503 Naghavi, M., Neal, B., Nelson, P. K., Nolla, J. M., Norman, R., Olives, C., Omer, S. B., Orchard, J., Osborne, R., Ostro,  
504 B., Page, A., Pandey, K. D., Parry, C. D. H., Passmore, E., Patra, J., Pearce, N., Pelizzari, P. M., Petzold, M., Phillips, M.  
505 R., Pope, D., Pope, C. A., Powles, J., Rao, M., Razavi, H., Rehfuess, E. A., Rehm, J. T., Ritz, B., Rivara, F. P., Roberts,  
506 T., Robinson, C., Rodriguez-Portales, J. A., Romieu, I., Room, R., Rosenfeld, L. C., Roy, A., Rushton, L., Salomon, J.  
507 A., Sampson, U., Sanchez-Riera, L., Sanman, E., Sapkota, A., Seedat, S., Shi, P., Shield, K., Shivakoti, R., Singh, G. M.,  
508 Sleet, D. A., Smith, E., Smith, K. R., Stapelberg, N. J. C., Steenland, K., Stöckl, H., Stovner, L. J., Straif, K., Straney, L.,  
509 Thurston, G. D., Tran, J. H., Van Dingenen, R., van Donkelaar, A., Veerman, J. L., Vijayakumar, L., Weintraub, R.,  
510 Weissman, M. M., White, R. A., Whiteford, H., Wiersma, S. T., Wilkinson, J. D., Williams, H. C., Williams, W., Wilson,  
511 N., Woolf, A. D., Yip, P., Zielinski, J. M., Lopez, A. D., Murray, C. J. L., and Ezzati, M.: A comparative risk assessment  
512 of burden of disease and injury attributable to 67 risk factors and risk factor clusters in 21 regions, 1990–2010: a  
513 systematic analysis for the Global Burden of Disease Study 2010[J], *Lancet.*, 380, 2224-2260,  
514 [https://doi.org/10.1016/S0140-6736\(12\)61766-8](https://doi.org/10.1016/S0140-6736(12)61766-8), 2012.

515 Liu, S., Liu, Z., Li, J., Wang, Y., Ma, Y., Sheng, L., Liu, H., Liang, F., Xin, G., and Wang, J.: Numerical simulation for the  
516 coupling effect of local atmospheric circulations over the area of Beijing, Tianjin and Hebei Province[J], *Sci. China Ser.*  
517 *D Earth Sci.*, 52, 382-392, <https://doi.org/10.1007/s11430-009-0030-2>, 2009.

518 Lu, C., Deng, Q.-h., Liu, W.-w., Huang, B.-l., and Shi, L.-z.: Characteristics of ventilation coefficient and its impact on urban  
519 air pollution[J], *J. Cent. South Univ.*, 19, 615-622, [10.1007/s11771-012-1047-9](https://doi.org/10.1007/s11771-012-1047-9), 2012.

520 Luo, M., Hou, X., Gu, Y., Lau, N.-C., and Yim, S. H.-L.: Trans-boundary air pollution in a city under various atmospheric  
521 conditions[J], *Sci. Total Environ.*, 618, 132-141, <https://doi.org/10.1016/j.scitotenv.2017.11.001>, 2018.

522 Luo, Y., Lu, D., Zhou, X., Li, W., and He, Q.: Characteristics of the spatial distribution and yearly variation of aerosol optical

523 depth over China in last 30 years[J], *J. Geophys. Res.*, 106, 14501-14513, <https://doi.org/10.1029/2001JD900030>, 2001.

524 MEP: China National Ambient Air Quality Standards, MEP, Beijing, China, 2012.

525 Miao, Y., Liu, S., Zheng, Y., Wang, S., Chen, B., Zheng, H., and Zhao, J.: Numerical study of the effects of local atmospheric  
526 circulations on a pollution event over Beijing–Tianjin–Hebei, China[J], *J. Environ. Sci.*, 30, 9-20,  
527 <https://doi.org/10.1016/j.jes.2014.08.025>, 2015.

528 Ni, C., Li, G., and Xiong, X.: Analysis of a vortex precipitation event over Southwest China using AIRS and in situ  
529 measurements[J], *Adv. Atmos. Sci.*, 34, 559-570, <https://doi.org/10.1007/s00376-016-5262-4>, 2017.

530 Ning, G., Wang, S., Ma, M., Ni, C., Shang, Z., Wang, J., and Li, J.: Characteristics of air pollution in different zones of  
531 Sichuan Basin, China[J], *Sci. Total Environ.*, 612, 975-984, <https://doi.org/10.1016/j.scitotenv.2017.08.205>, 2018.

532 Peng, X., and Cheng, L.: A case numerical study on the evolution of the plateau-east-side low vortex and shear line. Part  
533 I: Analysis and diagnosis[J], *J. Lanzhou Univ. Nat. Sci.*, 28, 163-168,  
534 <https://doi.org/10.13885/j.issn.0455-2059.1992.02.029>, 1992.

535 Qu, Y., Han, Y., Wu, Y., Gao, P., and Wang, T.: Study of PBLH and its correlation with particulate matter from one-year  
536 observation over Nanjing, Southeast China[J], *Remote Sens.*, 9, 668, 2017.

537 Quan, J., Gao, Y., Zhang, Q., Tie, X., Cao, J., Han, S., Meng, J., Chen, P., and Zhao, D.: Evolution of planetary boundary  
538 layer under different weather conditions, and its impact on aerosol concentrations[J], *Particuology.*, 11, 34-40,  
539 <https://doi.org/10.1016/j.partic.2012.04.005>, 2013.

540 Shi, Y., Zhang, N., Gao, J., Li, X., and Cai, Y.: Effect of fireworks display on perchlorate in air aerosols during the Spring  
541 Festival[J], *Atmos. Environ.*, 45, 1323-1327, <https://doi.org/10.1016/j.atmosenv.2010.11.056>, 2011.

542 Slingo, J. M.: The development and verification of a cloud prediction scheme for the ECWMF Model[J], *Q. J. Roy. Meteor.*  
543 *Soc.*, 113, 899-927, <https://doi.org/10.1002/qj.49711347710>, 1987.

544 Tang, G., Zhu, X., Hu, B., Xin, J., Wang, L., Münkler, C., Mao, G., and Wang, Y.: Impact of emission controls on air quality in  
545 Beijing during APEC 2014: Lidar ceilometer observations[J], *Atmos. Chem. Phys.*, 15, 743-750,  
546 <https://doi.org/10.5194/acp-15-12667-2015>, 2015.

547 Tao, J., Cheng, T., Zhang, R., Cao, J., Zhu, L., Wang, Q., Luo, L., and Zhang, L.: Chemical composition of PM<sub>2.5</sub> at an urban  
548 site of Chengdu in southwestern China[J], *Adv. Atmos. Sci.*, 30, 1070-1084, <https://doi.org/10.1007/s00376-012-2168-7>,  
549 2013a.

550 Tao, J., Zhang, L., Engling, G., Zhang, R., Yang, Y., Cao, J., Zhu, C., Wang, Q., and Luo, L.: Chemical composition of PM<sub>2.5</sub>  
551 in an urban environment in Chengdu, China: Importance of springtime dust storms and biomass burning[J], *Atmos. Res.*,  
552 122, 270-283, <https://doi.org/10.1016/j.atmosres.2012.11.004>, 2013b.

553 Tao, M., Chen, L., Su, L., and Tao, J.: Satellite observation of regional haze pollution over the North China Plain[J], *J.*  
554 *Geophys. Res.-Atmos.*, 117, n/a-n/a, 10.1029/2012JD017915, 2012.

555 Tao, M., Chen, L., Xiong, X., Zhang, M., Ma, P., Tao, J., and Wang, Z.: Formation process of the widespread extreme haze  
556 pollution over northern China in January 2013: Implications for regional air quality and climate[J], *Atmos. Environ.*, 98,  
557 417-425, <https://doi.org/10.1016/j.atmosenv.2014.09.026>, 2014.

558 Tian, P., Cao, X., Zhang, L., Sun, N., Sun, L., Logan, T., Shi, J., Wang, Y., Ji, Y., Lin, Y., Huang, Z., Zhou, T., Shi, Y., and  
559 Zhang, R.: Aerosol vertical distribution and optical properties over China from long-term satellite and ground-based  
560 remote sensing[J], *Atmos. Chem. Phys.*, 17, 2509-2523, <https://doi.org/10.5194/acp-17-2509-2017>, 2017.

561 Wang, Q.-W., and Tan, Z.-M.: Multi-scale topographic control of southwest vortex formation in Tibetan Plateau region in an  
562 idealized simulation[J], *J. Geophys. Res.-Atmos.*, 119, 11,543-511,561, <https://doi.org/10.1002/2014JD021898>, 2014.

563 Wang, T., Nie, W., Gao, J., Xue, L. K., Gao, X. M., Wang, X. F., Qiu, J., Poon, C. N., Meinardi, S., Blake, D., Wang, S. L.,  
564 Ding, A. J., Chai, F. H., Zhang, Q. Z., and Wang, W. X.: Air quality during the 2008 Beijing Olympics: secondary  
565 pollutants and regional impact[J], *Atmos. Chem. Phys.*, 10, 7603-7615, <https://doi.org/10.5194/acp-10-7603-2010>,  
566 2010.

567 Wang, X., Dickinson, R. E., Su, L., Zhou, C., and Wang, K.: PM<sub>2.5</sub> pollution in China and how it has been exacerbated by  
568 terrain and meteorological conditions[J], *Bull. Am. Meteorol. Soc.*, 99, 105-119,  
569 <http://dx.doi.org/10.1175/BAMS-D-16-0301.1>, 2018.

570 Wang, Y., Hao, J., McElroy, M. B., Munger, J. W., Ma, H., Chen, D., and Nielsen, C. P.: Ozone air quality during the 2008  
571 Beijing Olympics: Effectiveness of emission restrictions[J], *Atmos. Chem. Phys.*, 9, 5237-5251,  
572 <https://doi.org/10.5194/acp-9-5237-2009>, 2009.

573 Wang, Y., Yao, L., Wang, L., Liu, Z., Ji, D., Tang, G., Zhang, J., Sun, Y., Hu, B., and Xin, J.: Mechanism for the formation of  
574 the January 2013 heavy haze pollution episode over central and eastern China[J], *Sci. China Earth. Sci.*, 57, 14-25,  
575 <https://doi.org/10.1007/s11430-013-4773-4>, 2014.

576 Wang, Y., Zhuang, G., Xu, C., and An, Z.: The air pollution caused by the burning of fireworks during the lantern festival in  
577 Beijing[J], *Atmos. Environ.*, 41, 417-431, <https://doi.org/10.1016/j.atmosenv.2006.07.043>, 2007.

578 Wei, P., Cheng, S., Li, J., and Su, F.: Impact of boundary-layer anticyclonic weather system on regional air quality[J], *Atmos.*  
579 *Environ.*, 45, 2453-2463, <https://doi.org/10.1016/j.atmosenv.2011.01.045>, 2011.

580 Whiteman, C. D., Hoch, S. W., Horel, J. D., and Charland, A.: Relationship between particulate air pollution and  
581 meteorological variables in Utah's Salt Lake Valley[J], *Atmos. Environ.*, 94, 742-753,  
582 <https://doi.org/10.1016/j.atmosenv.2014.06.012>, 2014.

583 Wu, P., Ding, Y., and Liu, Y.: Atmospheric circulation and dynamic mechanism for persistent haze events in the  
584 Beijing–Tianjin–Hebei region[J], *Adv. Atmos. Sci.*, 34, 429-440, <https://doi.org/10.1007/s00376-016-6158-z>, 2017.

585 Yang, L., Wu, Y., Davis, J. M., and Hao, J.: Estimating the effects of meteorology on PM<sub>2.5</sub> reduction during the 2008  
586 Summer Olympic Games in Beijing, China[J], *Front Environ Sci Eng.*, 5, 331,  
587 <https://doi.org/10.1007/s11783-011-0307-5>, 2011.

588 Ye, X., Song, Y., Cai, X., and Zhang, H.: Study on the synoptic flow patterns and boundary layer process of the severe haze  
589 events over the North China Plain in January 2013[J], *Atmos. Environ.*, 124, 129-145,  
590 <https://doi.org/10.1016/j.atmosenv.2015.06.011>, 2016.

591 Yu, S., Gao, W., Xiao, D., and Peng, J.: Observational facts regarding the joint activities of the southwest vortex and plateau  
592 vortex after its departure from the Tibetan Plateau[J], *Adv. Atmos. Sci.*, 33, 34-46,

593 <https://doi.org/10.1007/s00376-015-5039-1>, 2016.

594 Zeng, S., and Zhang, Y.: The effect of meteorological elements on continuing heavy air pollution: A case study in the  
595 Chengdu area during the 2014 Spring Festival[J], *Atmosphere.*, 8, 71, <https://doi.org/10.3390/atmos8040071>, 2017.

596 Zhang, J., Luo, B., Zhang, J., Ouyang, F., Song, H., Liu, P., Cao, P., Schäfer, K., Wang, S., Huang, X., and Lin, Y.: Analysis  
597 of the characteristics of single atmospheric particles in Chengdu using single particle mass spectrometry[J], *Atmos.*  
598 *Environ.*, 157, 91-100, <https://doi.org/10.1016/j.atmosenv.2017.03.012>, 2017.

599 Zhang, J. P., Zhu, T., Zhang, Q. H., Li, C. C., Shu, H. L., Ying, Y., Dai, Z. P., Wang, X., Liu, X. Y., Liang, A. M., Shen, H. X.,  
600 and Yi, B. Q.: The impact of circulation patterns on regional transport pathways and air quality over Beijing and its  
601 surroundings[J], *Atmos. Chem. Phys.*, 12, 5031-5053, <https://doi.org/10.5194/acp-12-5031-2012>, 2012a.

602 Zhang, S.-T., and Niu, S.-J.: Haze-to-fog transformation during a long lasting, low visibility episode in Nanjing[J], *J. Trop.*  
603 *Meteorol.*, 22, 67-77, <https://doi.org/10.16555/j.1006-8775.2016.S1.007>, 2016.

604 Zhang, X. Y., Wang, Y. Q., Niu, T., Zhang, X. C., Gong, S. L., Zhang, Y. M., and Sun, J. Y.: Atmospheric aerosol  
605 compositions in China: Spatial/temporal variability, chemical signature, regional haze distribution and comparisons  
606 with global aerosols[J], *Atmos. Chem. Phys.*, 12, 779-799, <https://doi.org/10.5194/acp-12-779-2012>, 2012b.

607 Zhang, Z., Zhang, X., Gong, D., Kim, S. J., Mao, R., and Zhao, X.: Possible influence of atmospheric circulations on winter  
608 haze pollution in the Beijing–Tianjin–Hebei region, northern China[J], *Atmos. Chem. Phys.*, 16, 561-571,  
609 <https://doi.org/10.5194/acp-16-561-2016>, 2016.

610

611



612 **Table 1.** Overview of the eight heavy air pollution events affected by dry low-pressure systems.  
 613

Event	Most polluted city	Heavy air pollution event		Most polluted day		End date of heavy air pollution event		Other cities with heavy air pollution
		Start and end dates of air pollution event	PM <sub>10</sub> concentration range in this period ( $\mu\text{g m}^{-3}$ )	Date	PM <sub>10</sub> concentration ( $\mu\text{g m}^{-3}$ )	Date	PM <sub>10</sub> concentration ( $\mu\text{g m}^{-3}$ )	
1	Mianyang	13–14 Jan 2006	284–442	13 Jan 2006	442	15 Jan 2006	166	Chengdu
2	Chengdu	29 Jan 2006	407	29 Jan 2006	407	30 Jan 2006	190	None
3	Chengdu	19–23 Dec 2006	348–385	23 Dec 2006	385	24 Dec 2006	246	None
4	Chengdu	21–24 Dec 2007	260–529	23 Dec 2007	529	25 Dec 2007	174	Mianyang
5	Chengdu	18–20 Jan 2009	264–381	19 Jan 2009	381	21 Jan 2009	220	Mianyang
6	Chengdu	3 Feb 2011	403	3 Feb 2011	403	4 Feb 2011	190	None
7	Chengdu	22–31 Jan 2014	282–562	31 Jan 2014	562	1 Feb 2014	207	Deyang
8	Chengdu	1–6 Jan 2017	294–480	5 Jan 2017	480	7 Jan 2017	118	Deyang

614  
 615  
 616  
 617  
 618

**Table 2.** Relative vorticity at 700 hPa during the periods of deteriorating and improving air quality in each of the eight heavy air pollution events.

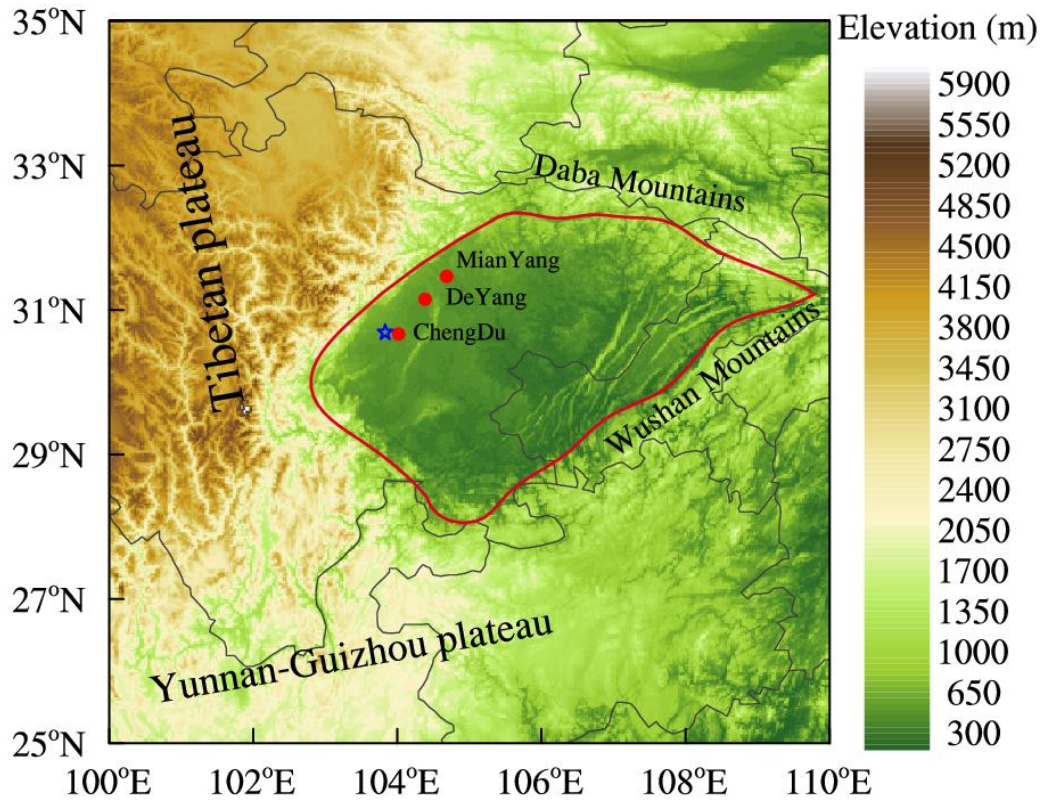
Event	Deteriorating air quality		Improving air quality	
	Time (BST)	Relative vorticity ( $1 \times 10^{-5} \text{ s}^{-1}$ )	Time (BST)	Relative vorticity ( $1 \times 10^{-5} \text{ s}^{-1}$ )
1	02:00 on 13 Jan 2006	2.58	20:00 on 13 Jan 2006	-0.94
2	02:00 on 29 Jan 2006	4.15	08:00 on 30 Jan 2006	-3.36
3	20:00 on 22 Dec 2006	4.64	14:00 on 23 Dec 2006	-1.09
4	14:00 on 22 Dec 2007	0.59	14:00 on 23 Dec 2007	-0.82
5	02:00 on 19 Jan 2009	1.75	08:00 on 19 Jan 2009	-2.48
6	02:00 on 3 Feb 2011	2.96	14:00 on 3 Feb 2011	3.16
7	02:00 on 31 Jan 2014	9.12	02:00 on 1 Feb 2014	5.49
8	20:00 on 4 Jan 2017	6.49	08:00 on 5 Jan 2017	-5.74

619  
 620

621 **Table 3.** Height of the atmospheric boundary layer (BLH), lower tropospheric stability (LTS), and mean wind speed  
622 (MWS) in the lower troposphere during periods of deteriorating air quality in each of the eight heavy air pollution  
623 events, and the differences of them between periods of improving and deteriorating air quality in each event.  
624

Event	Deteriorating air quality			Differences between periods of improving and deteriorating air quality		
	BLH (m)	LTS (K)	MWS ( $\text{m s}^{-1}$ )	BLH (m)	LTS (K)	WMS ( $\text{m s}^{-1}$ )
1	278.16	23.13	2.86	144.75	-11.23	0.41
2	375.42	29.45	4.12	139.08	-10.2	1.93
3	279.50	18.54	2.99	-16.45	-5.61	0.34
4	282.61	18.58	1.91	-39.62	-7.23	1.04
5	251.53	19.63	3.11	51.17	-7.88	0.85
6	282.16	25.80	4.22	-16.87	0.55	1.91
7	232.57	25.95	4.21	30.77	-1.97	-1.07
8	266.23	18.88	2.59	107.57	-8.4	0.27

625  
626



628

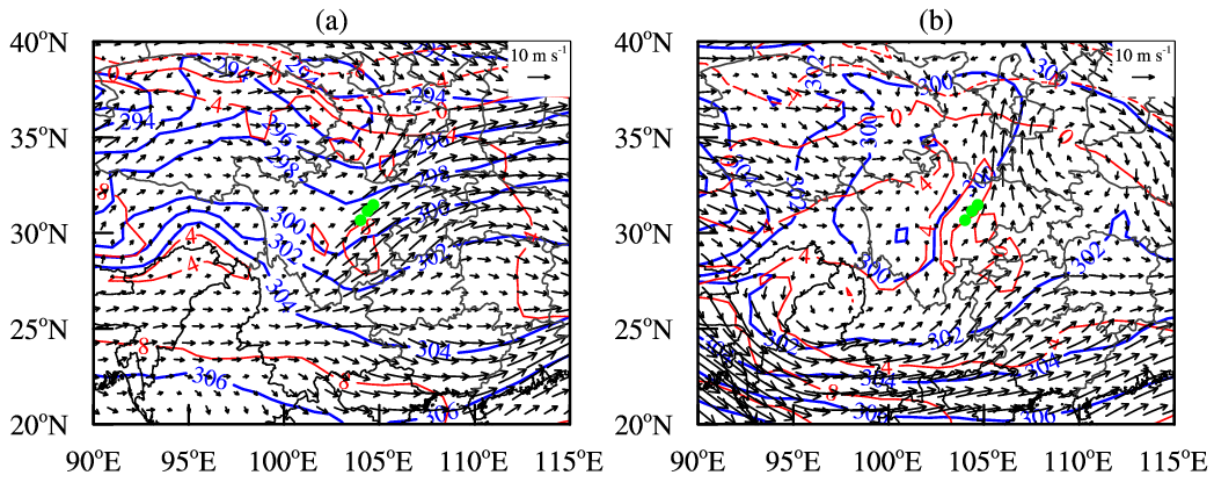
629

630

631

632

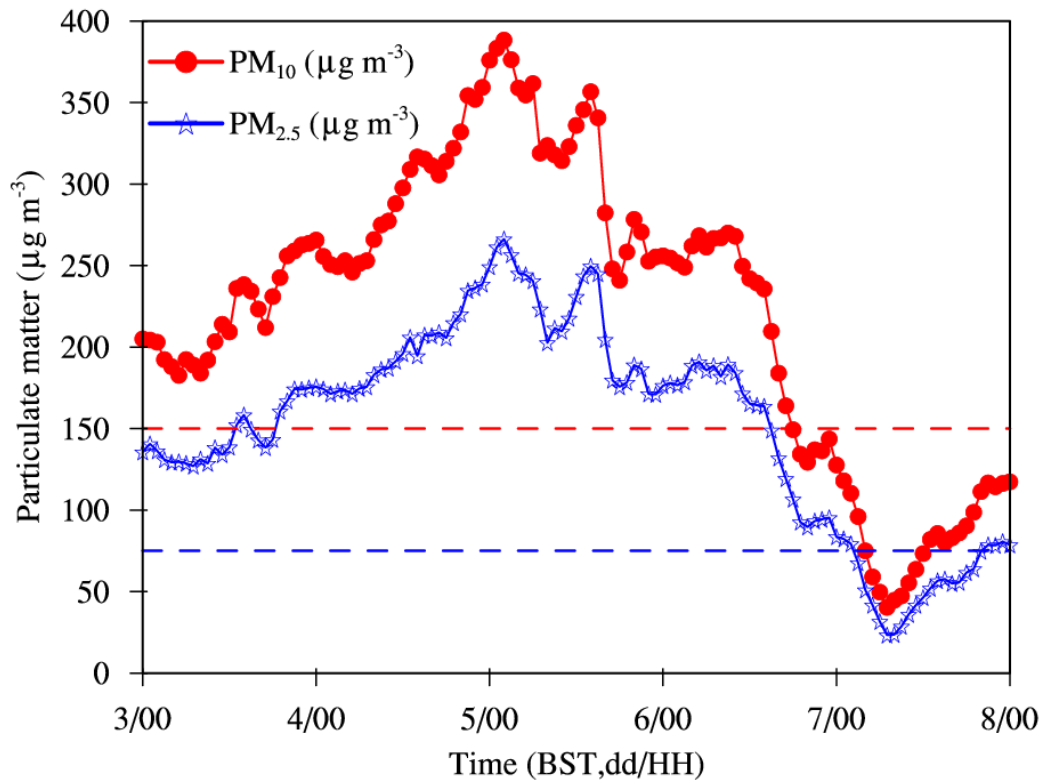
**Fig. 1** Topographic map (shading, units: m) of the Sichuan Basin (delineated in red) and surrounding areas showing the location of the cities of Chengdu, Deyang, and Mianyang (red dots). The Wenjiang station is marked with blue five-pointed stars. For interpretation of the colors, see web version of this article.



634

635 **Fig. 2** Weather maps at 700 hPa based on ERA-Interim daily data showing (a) a trough from event 2 at 20:00 BST on  
 636 28 January, 2006 and (b) a low vortex from event 4 at 14:00 BST on 22 December, 2007. The blue lines are isopleths  
 637 of geopotential height, the red lines are isotherms and the black arrows are wind vectors. The green dots show the  
 638 location of the urban agglomeration.

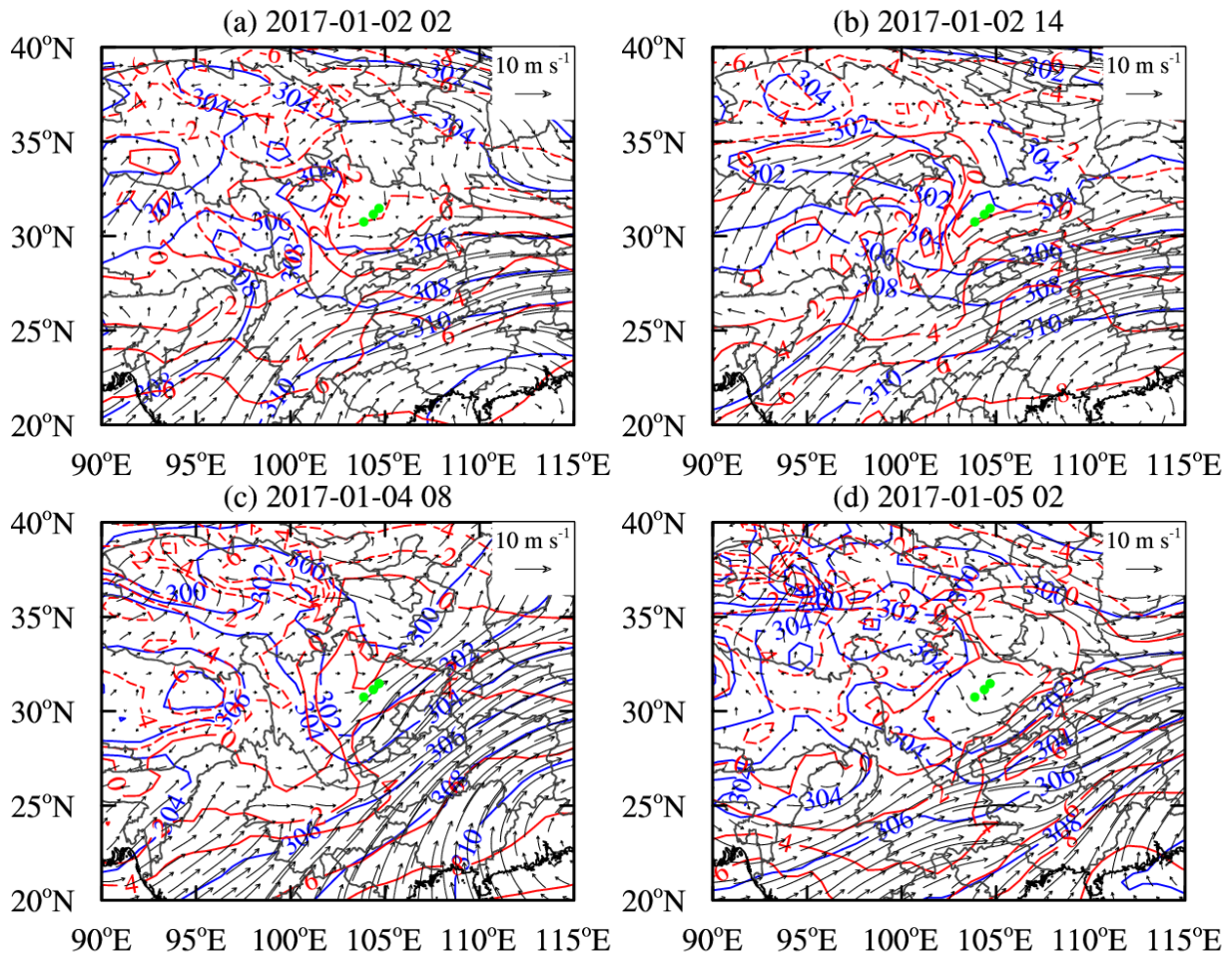
639



641

642 **Fig. 3** Average hourly concentrations of surface PM<sub>10</sub> (red solid line) and PM<sub>2.5</sub> (blue solid line) in the urban  
 643 agglomeration from 00:00 BST on 3 January 2017 to 00:00 BST on 8 January 2017 during event 8. The dashed red  
 644 line represents Grade II standard of PM<sub>10</sub> daily concentration ( $150 \mu\text{g m}^{-3}$ ), the dashed blue line represents Grade II  
 645 standard of PM<sub>2.5</sub> daily concentration ( $75 \mu\text{g m}^{-3}$ ).

646



648

649

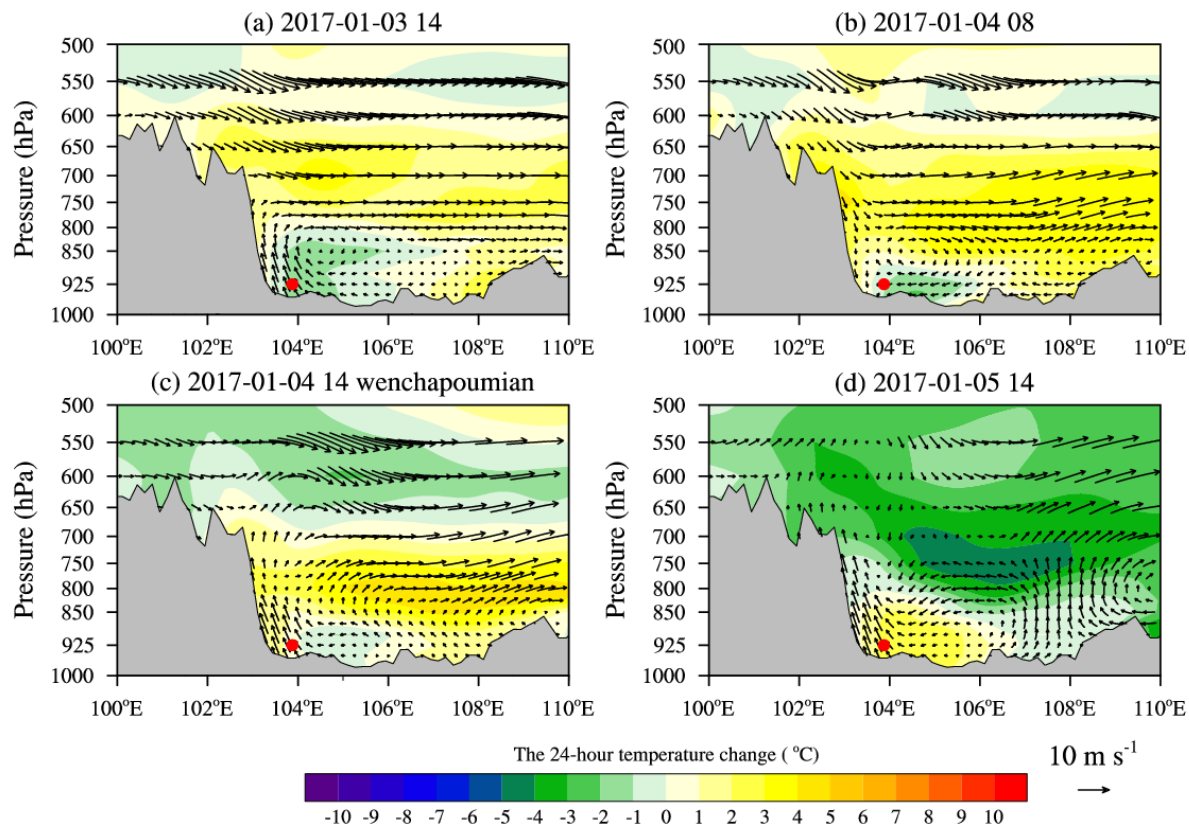
650

651

652

653

**Fig. 4** Weather maps at 700 hPa for event 8 at (a) 02:00 BST on 2 January 2017, (b) 14:00 BST on 2 January 2017, (c) 08:00 BST on 4 January 2017 and (d) 02:00 BST on 5 January 2017. The blue lines are isopleths of geopotential height, the red lines are isotherms and the black arrows are wind vectors. The green dots show the location of the urban agglomeration.

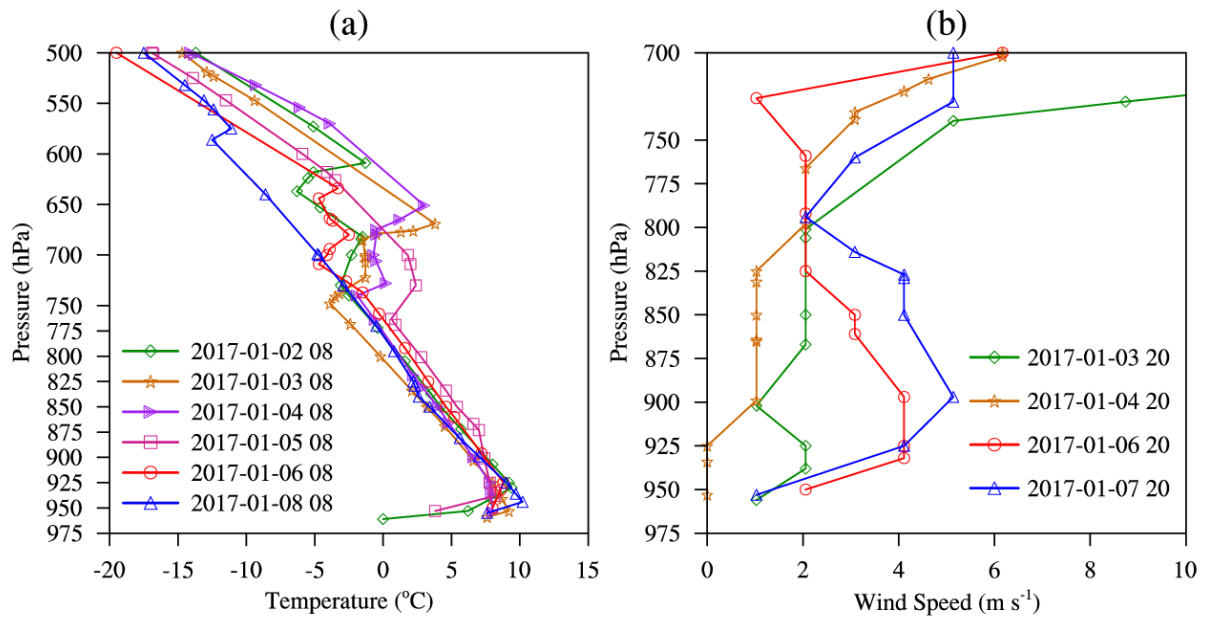


655

656 **Fig. 5** West-to-east vertical cross-sections of 24-hour temperature change (shading, units: °C) and wind vectors  
 657 (synthesized by u and w) through the most polluted area (30.75 °N) during event 8 at (a) 14:00 BST on 3 January 2017,  
 658 (b) 08:00 BST on 4 January 2017, (c) 14:00 BST on 4 January 2017 and (d) 14:00 BST on 5 January 2017 during  
 659 event 8. Note that the vertical velocity is multiplied by 100 when plotting the wind vectors. The most polluted area is  
 660 marked by red solid dots. The gray shading represents the terrain.

661

662



663

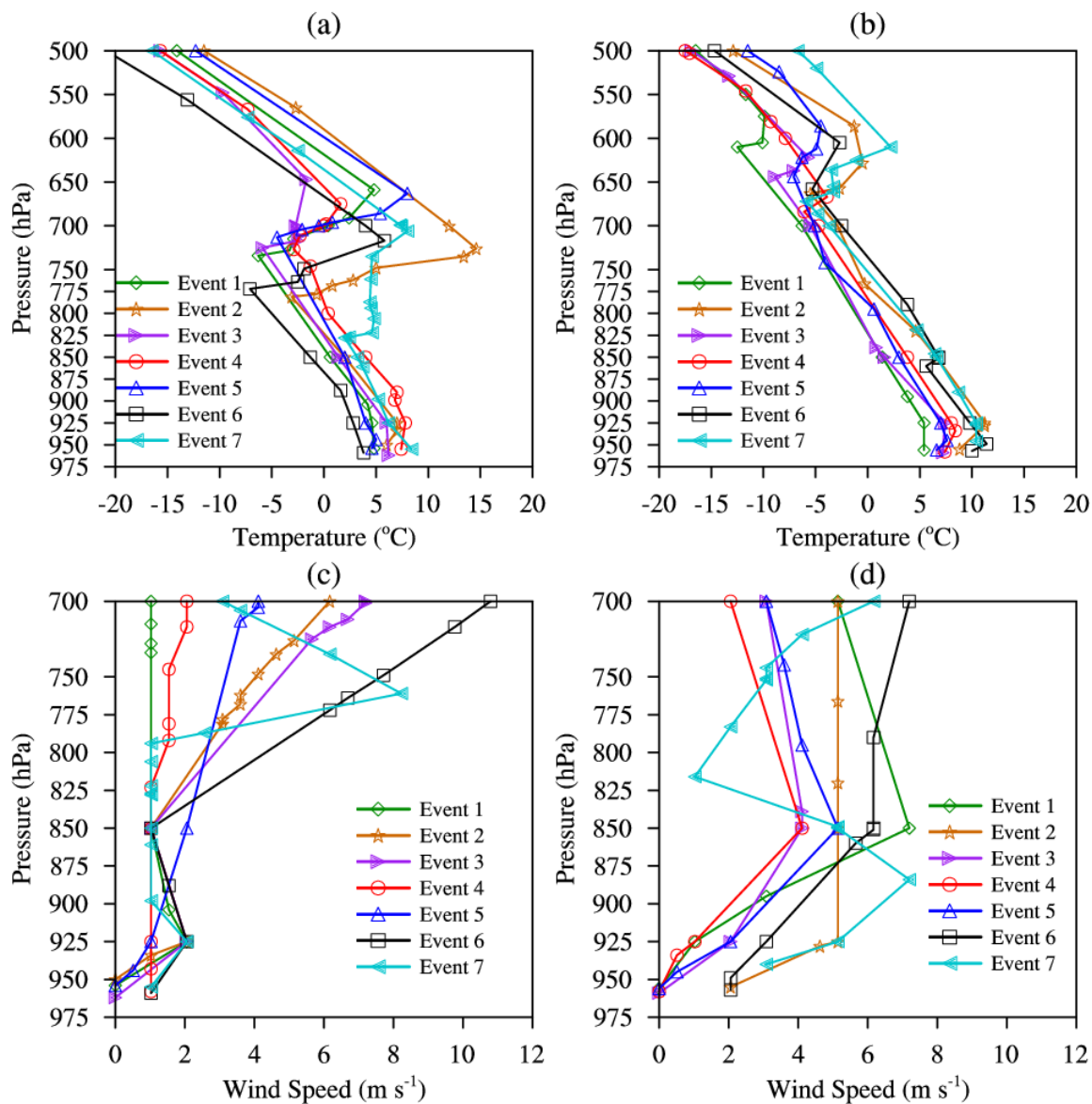
664

665

666

**Fig. 6** Vertical profiles of (a) temperature and (b) horizontal wind speed at Wenjiang station (30.75 °N, 103.875 °E, see **Fig. 1**) measured by radiosonde during event 8.

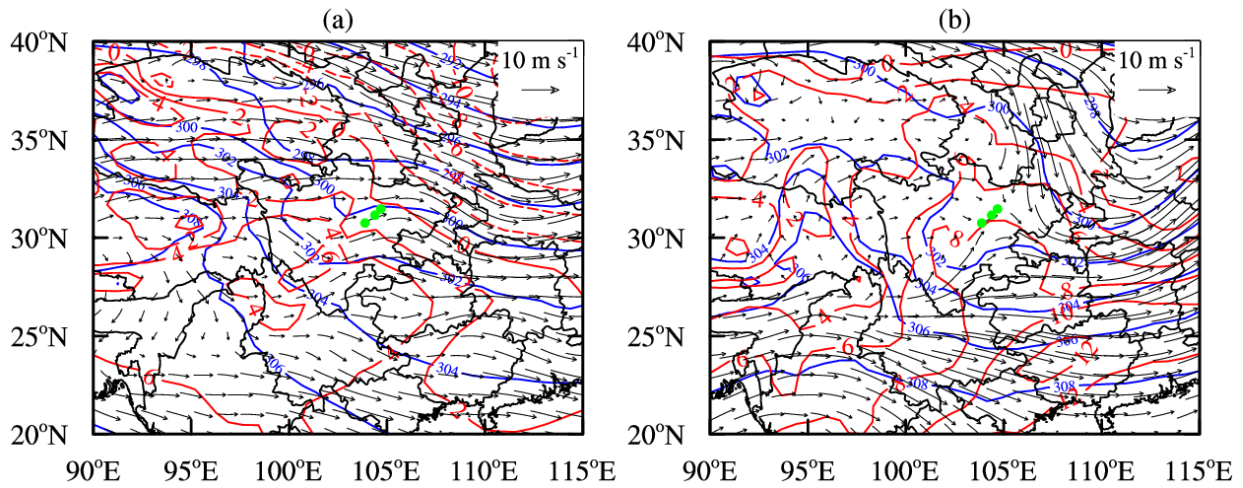




668

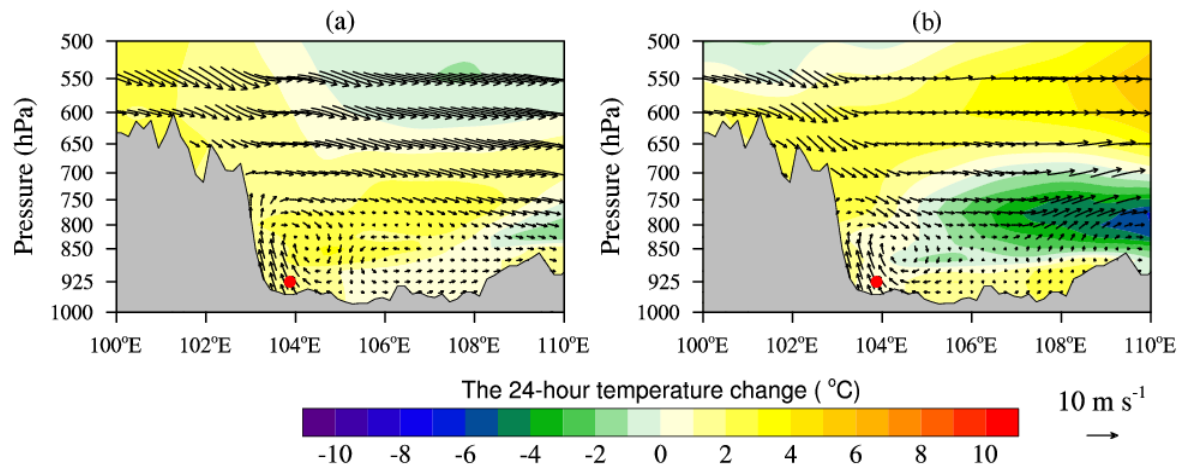
669 **Fig. 7** Vertical profiles of (a) temperature and (c) horizontal wind speed in the urban agglomeration during periods  
 670 controlled by the low-pressure system. Vertical profiles of (b) temperature and (d) horizontal wind speed after the  
 671 low-pressure system had transited across the urban agglomeration for seven heavy air pollution events (events 1–7).

672



673  
674  
675  
676

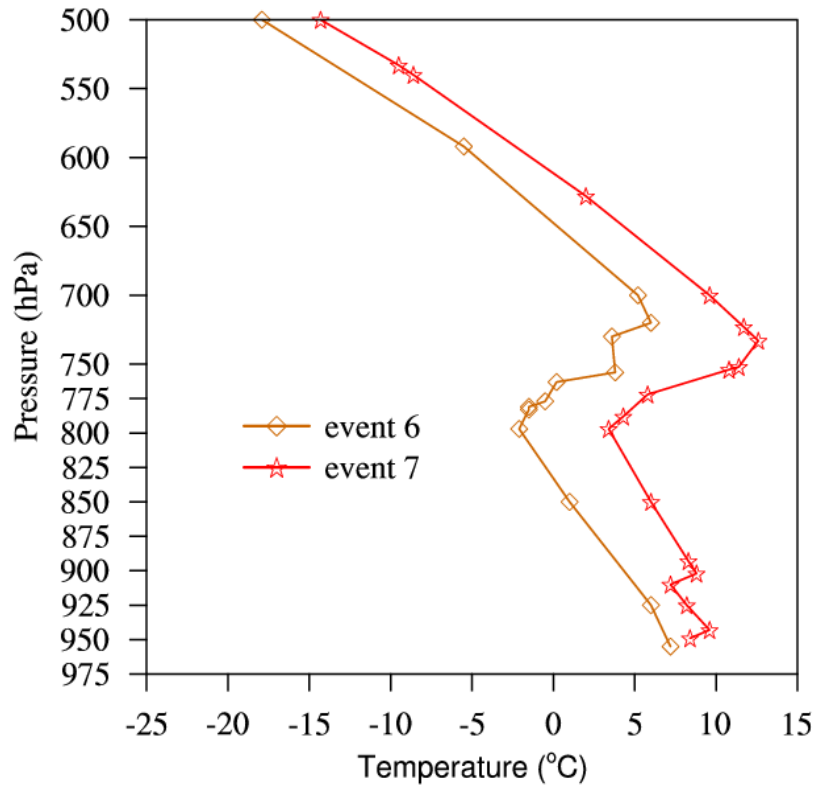
**Fig. 8** Weather maps at 700 hPa during periods of improving air quality (a) for event 6 and (b) for event 7. The blue lines are isopleths of geopotential height, the red lines are isotherms and the black arrows are wind vectors. The green dots show the location of the urban agglomeration.



678

679 **Fig. 9** West-to-east vertical cross-sections of 24-hour temperature change (shading, units: °C) and wind vectors  
 680 (synthesized by u and w) through the most polluted area (30.75 °N) during the periods of improving air quality (a) for  
 681 event 6 and (b) for event 7. Note that the vertical velocity is multiplied by 100 when plotting the wind vectors. The  
 682 most polluted area is marked by red solid dots. The gray shading represents the terrain.

683

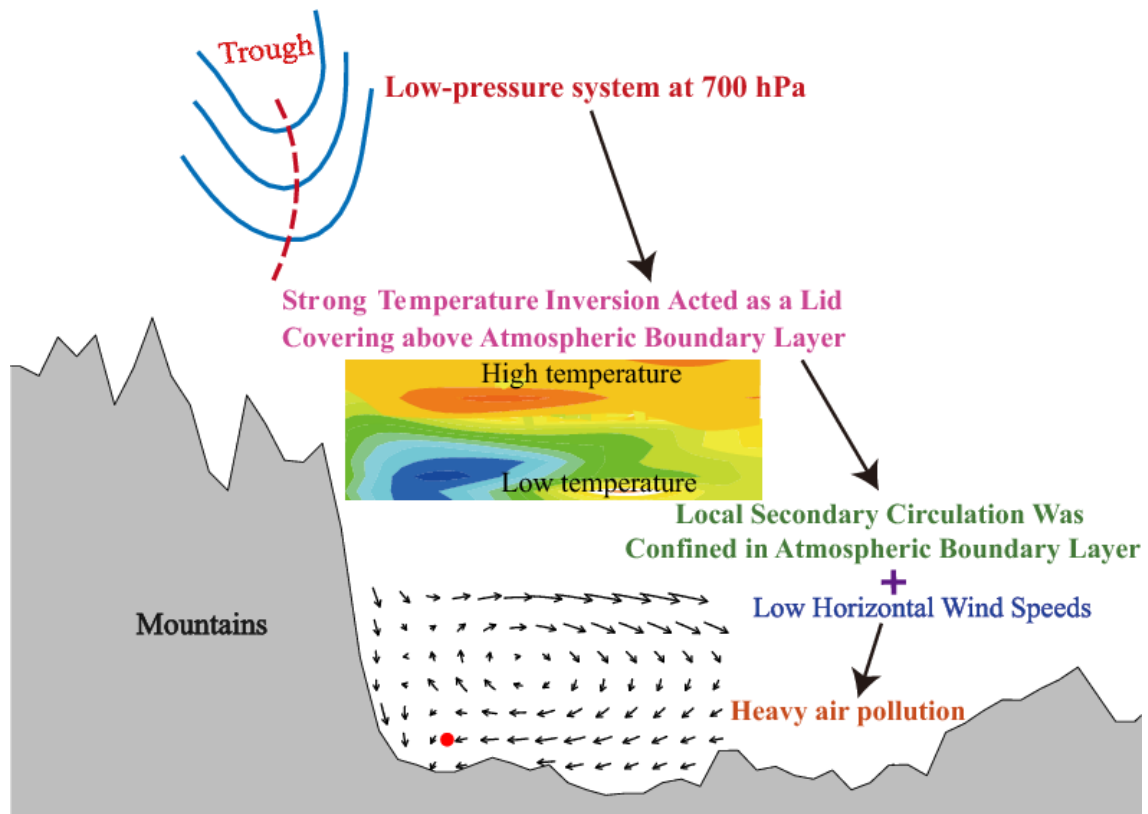


685

686 **Fig. 10** Vertical profiles of temperature at Wenjiang station (30.75 °N, 103.875 °E) measured by radiosonde during  
 687 periods of improving air quality for event 6 and 7.

688

689



691

692 **Fig. 11** Schematic diagram of the mechanism of influence of a dry low-pressure system on winter heavy air pollution  
 693 events in the urban agglomeration.

694

695